RESEARCH ARTICLE

Key Points:

- Agricultural tile drainage considerably decreases the mean travel time of shallow subsurface water during the growing season
- Filtering of the natural heterogeneity via the artificially replumbed landscape results in a homogenization of the hydrologic response
- Integration along the river network reduces the influence of catchment spatial heterogeneity on the mean travel time

Correspondence to:
M. Danesh-Yazdi,
dane0049@umn.edu

Inferring changes in water cycle dynamics of intensively managed landscapes via the theory of time-variant travel time distributions

Mohammad Danesh-Yazdi[1], Efi Foufoula-Georgiou[1,2], Diana L. Karwan[3], and Gianluca Botter[4]

[1]Department of Civil, Environmental, and Geo-Engineering, St. Anthony Falls Laboratory and National Center for Earth-Surface Dynamics, University of Minnesota, Minneapolis, Minnesota, USA, [2]Department of Civil and Environmental Engineering, University of California, Irvine, California, USA, [3]Department of Forest Resources, University of Minnesota, St. Paul, Minnesota, USA, [4]Dipartimento di Ingegneria Civile, Edile e Ambientale, Università degli studi di Padova, Padua, Italy

Abstract Climatic trends and anthropogenic changes in land cover and land use are impacting the hydrology and water quality of streams at the field, watershed, and regional scales in complex ways. In poorly drained agricultural landscapes, subsurface drainage systems have been successful in increasing crop productivity by removing excess soil moisture. However, their hydroecological consequences are still debated in view of the observed increased concentrations of nitrate, phosphorus, and pesticides in many streams, as well as altered runoff volumes and timing. In this study, we employ the recently developed theory of time-variant travel time distributions within the StorAge Selection function framework to quantify changes in water cycle dynamics resulting from the combined climate and land use changes. Our results from analysis of a subbasin in the Minnesota River Basin indicate a significant decrease in the mean travel time of water in the shallow subsurface layer during the growing season under current conditions compared to the pre-1970s conditions. We also find highly damped year-to-year fluctuations in the mean travel time, which we attribute to the "homogenization" of the hydrologic response due to artificial drainage. The dependence of the mean travel time on the spatial heterogeneity of some soil characteristics as well as on the basin scale is further explored via numerical experiments. Simulations indicate that the mean travel time is independent of scale for spatial scales larger than approximately 200 km^2, suggesting that hydrologic data from larger basins may be used to infer the average of smaller-scale-driven changes in water cycle dynamics.

1. Introduction

Water cycle dynamics play a central role in the ecological and biogeochemical functioning of a watershed determining the water quality, sediment composition, and cycling of pollutants, nutrients, carbon, and nitrogen in its water bodies and floodplains. Human activities in recent decades have left their signatures on many watersheds around the world: from the contamination of the receiving water bodies due to nutrients, pesticides, and fine sediments [*Kladivko et al.*, 2001; *Kanwar et al.*, 2005; *Botter et al.*, 2006; *Schottler et al.*, 2014] to altered streamflow dynamics at many space and time scales [e.g., *Vorosmarty and Sahagian*, 2000; *Zhang and Schilling*, 2006; *Foufoula-Georgiou et al.*, 2015] to impaired aquatic systems [e.g., *Zedler*, 2003]. One particular human activity of global interest is the intensification of agriculture for food and energy production [e.g., *Tilman et al.*, 2011; *Tscharntke et al.*, 2012; *Gelfand et al.*, 2013]. In the midwestern U.S., the replacement of hay and small grains with row crops of corn and soybean since the 1970s [e.g., see *Foufoula-Georgiou et al.*, 2015, Figure 2] has been accompanied by expansion of artificial surface and subsurface drainage, and also conversion of forests and wetlands to agricultural lands [*Pavelis*, 1987; *Dahl*, 2000; *Fraser et al.*, 2001]. In addition to human-induced landscape alterations, climatic trends in the Midwest have also been documented, especially following the mid-1970s with warmer temperatures, earlier snowmelt, increased annual precipitation, and rainfall events of higher intensity and shorter duration [e.g., *Karl et al.*, 1996; *Groisman et al.*, 2004, 2012; *Villarini et al.*, 2011; *Higgins and Kousky*, 2013]. Acknowledging that both climatic trends and human actions modulate hydrologic change, which might cascade down to other environmental changes, the goal of this study is to provide a quantitative framework within which to study possible changes in the time scales of water cycling in the landscape before it is discharged to the streams.

Changes in the time scales of water transport are important as they modulate changes in chemical and bio-geochemical reactions affecting the quality of water entering the streams.

In agricultural landscapes with poorly drained soils and wet climate, a considerable portion of the water would remain undrained after a rainfall event. The resulting high soil moisture would impose stress on plants during the growing season by limiting the adequate aeration required for crop root development [*Spaling and Smit*, 1995]. Subsurface agricultural drainage systems can remove soil moisture above the field capacity, lowering the water table, reducing the excess water stress on plants, and allowing greater plant uptake of nutrients [*Zucker and Brown*, 1998; *Fraser et al.*, 2001] while at the same time facilitating earlier cultivation, orderly planting and harvesting, and timely tillage [*Jin et al.*, 2008]. However, several studies and long-standing debates discuss the direct and indirect effects of agricultural drainage (both surface and subsurface) from the hydrological, ecological, and economical viewpoints [e.g., see *Blann et al.*, 2009, and references therein]. For instance, nutrient loss due to subsurface drainage has been reported as a serious water quality concern in many regions [e.g., *Skaggs et al.*, 1994; *Tomer et al.*, 2003] mainly due to the potential to augment the loss of soluble nutrients and sediment by providing *extra pathways* for *fast* delivery of water and nutrients to streams [e.g., *Chapman et al.*, 2005; *Basu et al.*, 2011], as well as bypassing biological processes taking place in the riparian zone [e.g., *Clement et al.*, 2003]. As an example, Figure 1a depicts the nitrate delivery into surface water throughout the State of Minnesota, showing increased levels in the southern half of the Minnesota River Basin including the Redwood subba-sin. More than 80% of the delivered nitrate arises from the agricultural fields, and the elevated nitrate concentration in streams is partially attributed to the artificial drainage system, which is recognized as the most active pathway from cropland sources to streams [*Minnesota Pollution Control Agency (MPCA)*, 2013].

Extensive installment of drainage systems has undoubtedly changed the water cycle dynamics and replumbed the subsurface structure by introducing extra flow pathways, making the landscape now respond differently compared to the prealtered condition. However, the change in the time scale of water and nutrient transport in such managed landscapes is still poorly understood. Multiple approaches exist to estimate the water particles' travel times based on a linear system's response perspective, each with their own advantages and limitations. One widely used approach relates catchment streamflow and pre-cipitation tracer concentrations through a stationary convolution kernel with a predefined shape (e.g., exponential and gamma) representing the steady state travel time distribution (TTD) of that catchment. This method requires hydrochemical data that are seldom available for direct calibration of the TTD [e.g., *Hrachowitz et al.*, 2011] and the data should also be of high frequency for a long period of time so that the tail of the TTD (signifying long-term catchment behavior) can be appropriately estimated [*Seeger and Weiler*, 2014; *Kirchner*, 2016]. Second, spatially distributed physical models with mechanistic or semiempir-ical parameterizations of all water transport pathways have been developed to track the water particles through a spatial domain and compute their travel times [e.g., *Fiori and Russo*, 2013]. However, such mod-els are often computationally expensive and might suffer from the well-known equifinality problem as they include a large number of parameters which are not directly observable and need to be calibrated with limited data. In this study, we employ a third model type: a lumped, stochastic Lagrangian formula-tion of transport [e.g., *Botter et al.*, 2011; *van der Velde et al.*, 2012; *Harman*, 2015] to estimate the probabil-istic structure of TTDs by using the available hydrologic data measured at the watershed scale to best infer how water particles with different ages in storage are preferentially sampled by the discharge. The promise of this approach for such a study lies in its potential to incorporate the influence of exogenous factors that can significantly impact the TTDs, such as the land use land-cover (LULC) change considered here. Our analysis brings forward the possibility that a reduced complexity framework informed by real watershed conditions can provide insight on water cycle changes and prompt further data collection and analysis. Such insight provides a departure point for understanding nutrient cycling based on the resi-dence times of water in the landscape. We emphasize that this study is not intended to estimate the real travel times in our specific catchment by performing a goodness of fit to any particular time series. Instead, the goal is to infer a first-order estimate of the *relative changes* in travel time statistics in those landscapes undergoing substantial alterations in LULC.

The rest of this paper is organized as follows. Section 2 presents the theoretical framework of the time-variant TTDs using the StorAge Selection (SAS) function approach. Section 3 describes the study site and
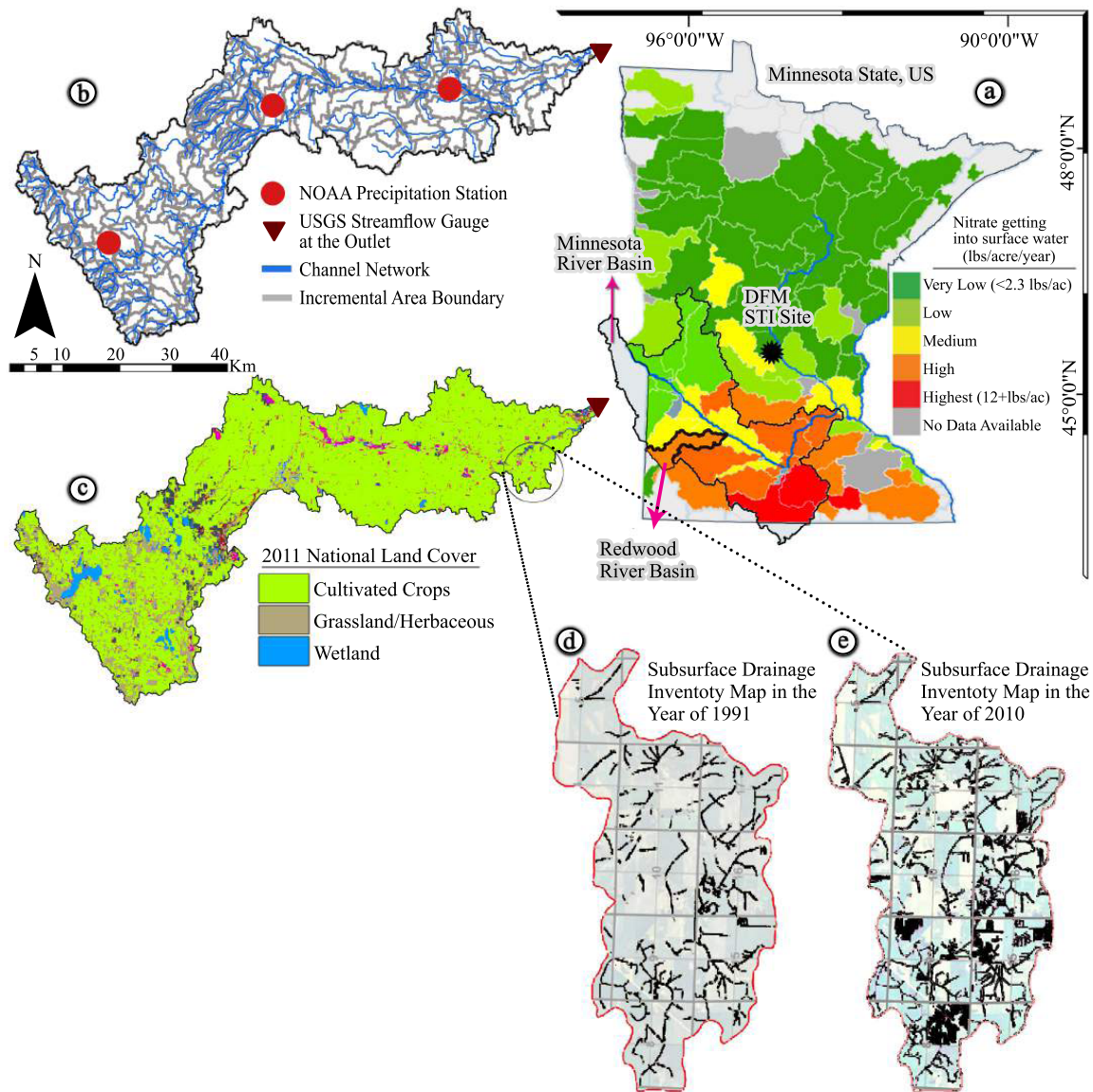
Figure 1. Land-cover, artificial drainage, and water quality in the Redwood River Basin. (a) Nitrate delivery into surface water throughout the Minnesota State, depicting increased levels in the southern half of the Minnesota River Basin (nitrate map produced by the Minnesota Pollution Control Agency) [*MPCA*, 2013]. (b) Map of the Redwood River Basin depicting channels and their incremental drainage areas. Daily precipitation data are available at three stations (Marshall, Vesta, and Tyler) marked with dots on the map and daily streamflow data are available at the outlet (USGS 05316500 Redwood River Station near Redwood Falls, MN). (c) The 2011 National Land Cover cropped lands (depicted by green pixels). Cropland sources account for an estimated 89–95% of the nitrate load in the Minnesota River Basin [*MPCA*, 2013]. (d and e) Subsurface drainage inventory maps of a part of the Redwood county in the years 1991 and 2010, respectively (produced by the Minnesota State University, Water Resources Center). The total length of subsurface tiles has been more than doubled in two decades, increasing the tile drainage density from 2.90 km^{-1} in 1991 to 6.34 km^{-1} in 2010.

data used in the analysis. A seasonal parameterization of the SAS function is proposed in section 4 to acknowledge the different mechanisms at play during the winter, snowmelt, growing, senescence, and fall periods, and a quantification of the TTDs during two periods of time: 1944–1976 (before LULC change denoted by BLUC) and 1976–2007 (after LULC change denoted by ALUC) is presented. Section 5 further investigates the dependence of the mean travel time (MTT) to the soil saturated hydraulic conductivity and the basin scale via numerical simulations. This is important since streamflow data are typically not available at plot scale but at much larger scales integrating the effects of the transport dynamics at the smaller scales of the watershed. Finally, section 6 concludes by summarizing the important findings.

2. Theory of Time-Variant Travel Time Distributions (TTDs): Concepts and Developments

2.1. Why Time-Variant TTDs?

The difference between a catchment's hydrologic response and TTD has been stressed by a number of studies [e.g., *Rodhe et al.*, 1996; *McGuire et al.*, 2005; *Heidbuchel et al.*, 2012]. The hydrologic response, controlled by the celerity of hydraulic potentials, reflects how fast a rainfall event is translated into discharge. In contrast, the TTD, controlled by the solute velocity, reflects the transport and aging of individual water particles during their travel in the catchment, which is time-variant and depends on the pore water velocity and history of prior precipitation and soil moisture [e.g., *McDonnell and Beven*, 2014]. Besides, the time scale of hydrologic response is often orders of magnitude smaller than the MTT of water because perturbations in the pressure head can advance much faster in the unsaturated soil profile than the transport of tracer or water particles through a catchment [*Kirchner et al.*, 2000; *Weiler et al.*, 2003; *Fiori and Russo*, 2008].

Due to the complex subsurface mixing mechanism and spatial heterogeneity in the preferential flow paths, proper quantification of the TTD is important for a better understanding and prediction of the water storage and solute transport in hydrologic systems [e.g., *McGuire et al.*, 2002; *Dusek et al.*, 2012; *Fiori and Russo*, 2013]. By using the concentration of a passive tracer or water stable isotope measured in the precipitation and streamflow, several studies have attempted to estimate the travel times by assuming and parameterizing a theoretical form for the TTD (see *McGuire and McDonnell* [2006] and references therein for a comprehensive review on the catchment travel time modeling). Such studies include investigating the role of topography [*McGuire et al.*, 2005; *Broxton et al.*, 2009; *Tetzlaff et al.*, 2009a], soil hydrology [*Soulsby et al.*, 2006; *Tetzlaff et al.*, 2009b; *Troch et al.*, 2013], climate [*Hrachowitz et al.*, 2009; *Heidbuchel et al.*, 2013], and geology [*Asano and Uchida*, 2012] on the mean travel or residence time by observation-based modeling. In many of these attempts, the assumed TTDs (such as the exponential or gamma distributions) are calibrated under the steady state assumption, i.e., water storage and hydrologic fluxes in the catchment do not change over time. However, this consideration is insufficient to account for the antecedent soil moisture condition and the temporal dynamics of the physical processes such as precipitation and evapotranspiration, which are the primary sources of temporal variability and irregular shape of the TTDs. In addition to these first-order controls, preferential contribution of aged water in the soil storage to the outfluxes (such as discharge and evapotranspiration) plays a second-order control which is driven by the catchment physical properties and spatiotemporal distribution of (in)active flow paths. The time-varying nature of the travel times is thus governed by both the temporal variability of the storage and hydrologic fluxes and the way different ages are sampled from the subsurface, which explains the distinction between different catchments in how they retain or release the water in storage.

2.2. Recent Developments in Formulating the Time-Variant TTDs

Several time-varying approaches have been developed so far to address the time-variant feature of the TTDs and advance our understanding of the dynamic response of catchments [*Hrachowitz et al.*, 2010b; *Roa-García and Weiler*, 2010; *Birkel et al.*, 2012; *McMillan et al.*, 2012; *Heidbuchel et al.*, 2012]. This study employs the recently developed theory of time-variant TTDs within the SAS function framework [*Botter et al.*, 2010, 2011; *van der Velde et al.*, 2012; *Harman*, 2015; *Benettin et al.*, 2015a] that explicitly accounts for the aforementioned major controls on the temporal dynamics of the TTDs. In what follows, we adopt the concepts presented in the study of *Botter et al.* [2010] and use the same notation for consistency.

By conceptualizing the catchment as a single control volume (CV) and assuming that the loss to and/or the recharge from groundwater is negligible, the major fluxes closing the mass balance for the water storage (S) in the CV are precipitation (J) as the only source of input, discharge (Q) at the outlet, and evapotranspiration (ET). The ET integrates the evaporation from the soil surface and the plant transpiration by accounting for the solar and terrestrial radiation, climatic attributes, plant type, and water availability. Using the Lagrangian description of flow, the time at which a given water particle enters and exits the CV is represented by t_i and t_e, respectively. The travel time (t_T) is then defined as $t_T = t_e - t_i$, i.e., the time spent by the particle since its entrance into the CV at time t_i until it exits the CV at time t_e. Correspondingly, the partition function, $\theta(t_i)$, is defined as the fraction of those particles injected at time t_i that will eventually join the stream as discharge. Alongside the travel time, the age or residence time (t_R) of a particle is defined as the elapsed time since the particle entered into the CV, i.e., $t_R = t - t_i$. Recently, *Benettin et al.* [2015a] provided

a coupled description of transport processes using life expectancy and travel time. The life expectancy (t_E) [*Cornaton and Perrochet*, 2006] is the time a particle is expected to spend from the current moment until it reaches the outlet, i.e., $t_E = t_e - t$. Therefore, it can be immediately concluded that the travel time of a particle is a special case of its age and life expectancy, i.e., the travel time is the same as life expectancy at time of injection while it coincides with the residence time when evaluated at the exit time.

By keeping track of each water particle and recording the corresponding travel and residence times, three types of time-relevant distributions can be constructed to characterize the particles transport in the CV. The *residence time distribution*, $p_R(t_R, t)$, is the probability distribution of the ages of all particles that are still present in the CV at time t. The set of residence times existing in the CV changes as time progresses due to the disproportional entrance of zero-age particles and exit of older ones, thereby the residence time distribution varies in time as well. Depending on whether the particles are tracked forward or backward in time, TTDs can be defined in two separate ways. The *TTD conditioned on the injection time*, $p_T(t_T, t_i)$, or the *forward TTD* gives the probability distribution of the travel time of those particles that were injected into the CV at the same time t_i. On the other hand, the *TTD conditioned on the exit time*, $p'_T(t_T, t_e)$, or *backward TTD*, represents the probability distribution of the ages of particles sampled in the discharge at time t_e, no matter when they entered into the CV. It is worth mentioning that in general, the forward and backward distributions are not necessarily the same except under the steady-steady condition when the water storage is constant [*Niemi*, 1977; *Rinaldo et al.*, 2011]. Moreover, the backward distribution is always constrained by the residence time distribution since the ages of particles in the discharge at any given time have to be a subset of the ages available in the CV at that time.

In order to derive explicit expressions for the residence time distribution, and forward and backward TTDs, three independent equations are needed [*Botter et al.*, 2011]. The first relationship known as the *Niemi*'s [1977] equation expresses the mass balance between the fraction of water particles injected at time t_i leaving the CV via Q at time t, and the fraction of the discharge sampled at time t composed of those particles entered at time t_i. The second equation, known as the master equation (ME), describes how the distribution of the ages of water particles changes over time. This equation is indeed a spatially integrated version of the general transport equation presented by *Benettin et al*. [2013a], which combines the fundamental formulation of transport (obeying the Fokker-Plank equation with a similar form to the advection-dispersion model) proposed by *Dagan* [1989] and the water age theory developed by *Ginn* [1999]. Finally, the third independent equation is given by writing the relationship between the backward and residence time distributions through the SAS function (see Appendix A for the expression of the above equations and analytical derivation of the residence and travel time distributions). These nonnegative time-dependent functions essentially describe how different ages available in storage are preferentially sampled by the discharge or other form of out-fluxes. The SAS function thus integrates the effects of heterogeneity in flow paths and dispersion mechanisms dictating the water and solute transport through a hydrologic system [*Benettin et al.*, 2013a; *Rinaldo et al.*, 2015] (see also Appendix B for more refined representations of the SAS functions).

As the explicit expressions show, the travel and residence time distributions are governed by (i) the temporal variability of the precipitation, evapotranspiration, discharge, and water storage in soil, and (ii) how the discharge and evapotranspiration SAS functions dictate the distribution of ages sampled by Q and ET, respectively, from the ages available in S. Even if the SAS function is treated as time-invariant, these distributions are still time-variant as they are directly dependent on the temporal dynamics of the above fluxes. In the context of the managed landscapes, it can also be recognized how the influence of altered soil hydrology and runoff generating mechanisms might be captured by the above controls on the TTDs. Transport through the artificial drainage systems, as strong preferential flow paths, bypasses the complex dispersion in the subsurface resulting in water and solute delivery to the streams much faster than they might naturally move within the soil matrix. This is directly expressed in the SAS function (as the second-order control on the TTD) by giving higher preference to the younger water particles while sampling different ages in the soil storage during those times that the drainage system is active. On the other hand, quick removal of excess moisture from the shallow subsurface layer by the drainage system leaves more vacant space in the soil, which prevents overland flow generation (via allowing higher infiltration) and decreases the chance of evaporation. The resulting change in the balance between these hydrologic fluxes in such "engineered landscapes" is explicitly reflected in the TTD as a first-order control. Quantification of change in the catchment TTDs undergone LULC alterations will be further explored in section 4.
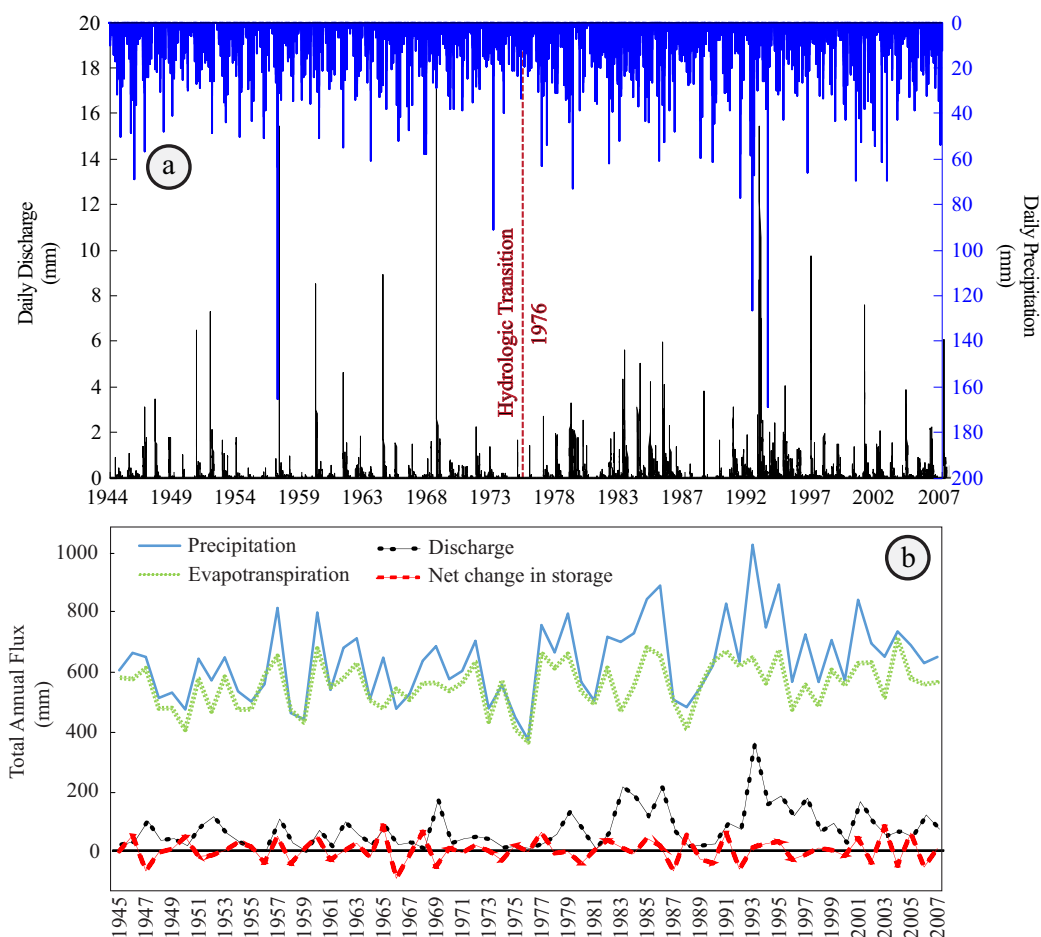
Figure 2. Hydrologic change in the Redwood River Basin. (a) Daily precipitation and streamflow time series for the Redwood basin from 1944 to 2007 with the hydrologic transition year of 1976 marked (see text). (b) Annual series of observed precipitation and streamflow and estimated evapotranspiration (see text) together with annual mass balance expressed as net change in storage.

3. Study Area and Data

3.1. Climate and Land Use

The 1821 km^2 Redwood River Basin (44°33′N, 95°40′W) is one of the main subbasins of the Minnesota River Basin located in the upper midwestern U.S. (Figure 1a). The basin, which ranges from 253 to 608 m above sea level in elevation, is underlain by Cretaceous sedimentary rocks and consists of soils that are primarily loamy sand within the Quaternary glacial till with scattered sandy outwash and silty alluvium on flood plains. The erodibility is moderate over the majority of the basin, having a complex mixture of well and poorly drained soils [*USDA-NRCS*, 2015]. The climate is continental with dry cold winters and wet warm summers. The average monthly temperature at the Redwood Falls over the 1944–2007 period fluctuates between −15.6°C in January and 16.4°C in July. The mean annual precipitation is 658 mm, more than 60% of which normally falls from May through September and there is almost no snow on ground during May– September. The average annual runoff is about 82 mm, and evapotranspiration is a sizable component of the annual water budget estimated to be approximately 80–90% of the total precipitation [e.g., *Minnesota Pollution Control Agency* (*MPCA*), 2007].

Agriculture is the main land use in this basin where approximately 82% of the total available area in 949 farm lands consists of row crops (Figure 1c). The cropping pattern has been significantly changed since 1940s with increasing rate of corn and soybean cultivation, currently covering nearly 86% of the cropped lands, while small grains, hay, and grasslands constitute the rest of the balance [*U.S. Department of Agriculture* (*USDA*), 2015; see also *Foufoula-Georgiou et al.*, 2015, Figure 2a]. Artificial subsurface drainage is a

common practice in this basin where the total length of subsurface tiles has been more than doubled in two decades (Figures 1d and 1e), increasing the tile drainage density (i.e., total length of tiles divided by the drainage area) from 2.90 km^{-1} in 1991 to 6.34 km^{-1} in 2010. Analysis of precipitation and streamflow data for the Redwood basin indicates that daily precipitation statistics have not changed significantly in the ALUC period except for increased daily rainfall amounts during November–February, while daily streamflow has increased consistently in all months. Moreover, Copula analysis of the daily rainfall and streamflows reveals sharper rising limbs of streamflow hydrographs and stronger dependence on the previous-day precipitation during the growing season of May–June, which has then been attributed to nonclimatic effects such as the extensive installment of surface diches and subsurface drainage tiles over the years in this watershed [*Foufoula-Georgiou et al.*, 2015].

3.2. Hydroclimatic Variables for Water Balance

In order to compute the TTDs, we need daily hydroclimatic data over our entire study period (1944–2007) including precipitation (rainfall and the water equivalent of any type of frozen precipitation), discharge, and evapotranspiration. The daily precipitation at three available National Oceanic and Atmospheric Association stations [NOAA, 2015], namely Marshall (GHCND: USC00215204), Vesta (GHCND: USC00218520), and Tyler (GHCND: USC00218429) for the 1944–2007 period is averaged to obtain a single precipitation signal for the basin, and the daily streamflow data are available at the USGS 05316500 Redwood River Station near Redwood Falls, MN (Figures 1b and 2a). The daily evapotranspiration is estimated as

$$ET(t) = RET \times K_c \times K_w(t) \tag{1}$$

where RET is the daily reference evapotranspiration estimated using the Penman-Monteith method [*Walter et al.*, 2001], K_c is the crop coefficient, and K_w is the water availability coefficient. RET is estimated by using the minimum and maximum temperatures measured at the same NOAA stations, but due to the lack of long-term solar radiation, wind speed, and dew point temperature data sets, the available data at the nearest stations in the Minnesota River Basin are used as surrogate for these climatic variables. Corn, soybean, and hay are considered as dominant crops to compute K_c, and the percentage of total area cultivated by these crops each year is also taken into account. The duration of each plant's different growing stages accompanied by the corresponding crop coefficients are chosen as those recommended by *Hinck* [2008] for Southern Minnesota. The crop planting and harvesting time during the study period is determined based on the data provided by *Cardwell* [1982] and the U.S. Department of Agriculture, National Agricultural Statistical Service [*USDA*, 2015] (see Appendix C for more detail). The crop planting time should be properly included to make sure evapotranspiration is turned on at the right time of a year. This affects our analysis because evapotranspiration can play a key role on restricting the fraction of the water particles joining the streamflow, thereby affecting the TTDs via the partition function. K_w is computed by using the empirical relationship proposed by *Holmes and Robertson* [1963] as

$$K_w(t) = \begin{cases} 1 & s(t) > s_{fc} \\ 0 & s(t) < s_{wp} \\ \dfrac{\ln\left(100\left(\dfrac{s(t)-s_{wp}}{s_{fc}-s_{wp}}\right)+1\right)}{\ln(101)} & s_{wp} < s(t) < s_{fc} \end{cases} \tag{2}$$

where $s(t)$ is the soil moisture content, and s_{wp} and s_{fc} are the moisture content at the wilting point and field capacity, respectively. s_{wp} and s_{fc} are set to 0.11 and 0.31, respectively, which are typical for loamy sand soils [*Laio et al.*, 2001]. Starting with an initial $s(t)$, $K_w(t)$ and the soil storage $S(t+1)$ are computed dynamically via solution of the mass balance equation (i.e., $dS(t)/dt = J(t) - Q(t) - ET(t)$) and equation (2), respectively, at a daily time step. The storage in a unit area of the shallow subsurface layer is equal to the product of the soil moisture content, soil porosity (set to 0.42 as the soil in the Redwood basin is mostly loamy sand), and the depth over which the soil storage is considered (set to 1.2 m which is the distance between the soil surface and the typical depth of drainage tiles being installed in this basin). It is noted that the assumed initial value for soil moisture content does not affect the results as its effect is dissipated after about 10 months and our analysis is performed over periods of approximately 64 years.

To provide confidence in our estimation of the daily evapotranspiration, we computed the annual change in storage as shown in Figure 2b, which indicates that the long-term average of the year-to-year fluctuations is very small (i.e., 1.08 mm) and no systemic trend is present in these fluctuations. Furthermore, average annual evapotranspiration constitutes 88% of the average annual precipitation (with a standard deviation of $\pm9.7\%$), which is in accordance with the previously reported budget for the Redwood basin by the *MPCA* [2007]. We also studied the sensitivity of the estimated *RET* to the air temperature, solar radiation, and wind speed. By changing these climatic variables each at a time by $\pm20\%$, the wind speed showed the smallest influence on the estimated long-term average daily *RET*, followed by the solar radiation and air temperature. The percent change in *RET* by varying the wind speed, solar radiation, and air temperature in the above range was (0.69, -0.61), (1.19, -4.98), and (2.48, -8.41), respectively.

4. Quantifying the Change in the Mean Travel Time (MTT)

The residence and travel time distributions are computed from equations (A5) to (A7) for the 1944–2007 period by using the daily time series of the hydrologic fluxes discussed in section 3, as well as the SAS functions parameterized by characterizing how water particles with different ages in the subsurface contribute to the discharge and evapotranspiration. For the Redwood River Basin, it was established in *Foufoula-Georgiou et al.* [2015] that 1975–1976 marked a year of significant hydrologic change partially impacted by tile drainage as inferred from simultaneous analysis of land cover data and localized multiscale decomposition of daily precipitation and corresponding streamflow time series using wavelets (see Figure 2a).

4.1. Parameterization of the StorAge Selection (SAS) Function
4.1.1. Qualitative Inference of the Type and Form of the SAS Functions
Availability of high-resolution hydrochemical data series for input and output fluxes is indispensable for determining the appropriate form of the SAS functions that describe the underlying sampling schemes of water ages in storage by the outfluxes [*van der Velde et al.*, 2014; *Harman*, 2015; *Queloz et al.*, 2015; *Benettin et al.*, 2015b]. Due to the lack of hydrochemical data in the Minnesota River Basin, however, direct estimation and calibration of the SAS function is infeasible. We use knowledge of hydrologic fluxes at daily time scales including precipitation, direct subsurface tile flow, soil moisture, and temperature data to construct representative and justifiable approximations of the sampling mechanism at different periods within a year in the BLUC and ALUC periods. This approach is described below for the Redwood basin.

For the evapotranspiration SAS function, the random-sampling scheme ($\omega_{ET} = 1$) is assumed for both the BLUC and ALUC periods, consistent with documented *ET* age sampling formulations in basins with wet climatic conditions [*van der Velde et al.*, 2014]. However, different types of the discharge SAS functions (ω_Q) are assumed for the BLUC and ALUC periods and also during distinct seasons of the year to account for various sampling schemes of those water particles leaving the system as discharge, depending on the climatic condition, loss due to evapotranspiration, and soil moisture dynamics. To infer the form of the discharge SAS function (ω_Q) in the ALUC period, we used hydrologic data from the 11.41 ha monitoring site, ST1, near the Redwood basin (see Figure 1a) operated by the Discovery Farms Minnesota (DFM) program, where 15 min measurements of subsurface tile drainage flow and soil moisture are available (Discovery Farms Minnesota, Hydro-climate data at Stearns, Dodge, and Blue Earth Sites, Minnesota, personal communication, 2015). By mutual comparison of the precipitation, subsurface tile drainage discharge, and soil moisture time series, some inferences about the mixing processes in the subsurface root zone layer are made, which then help to parameterize the SAS functions. Figure 3 shows these data for the water year 2013, which are representative of the data available for other water years (2012–2015) with respect to runoff ratio, planting and harvesting times, and the period over which drainage from tiles was observed.

1. *Winter season* (*December–March*). According to the temperature data, the soil surface is almost always frozen during December–March and precipitation accumulates as snow. Since the excess soil moisture was already removed by the drainage tiles prior to freezing and no new water can infiltrate into the subsurface, streamflow during this season does not consist of water particles draining from the shallow subsurface layer. This is consistent with the observation showing that the soil moisture is much less than the field capacity and no direct subsurface tile drainage is recorded during this period (Figure 3b). Thus the discharge SAS function in these months is formulated such that higher preference is given to the older particles.
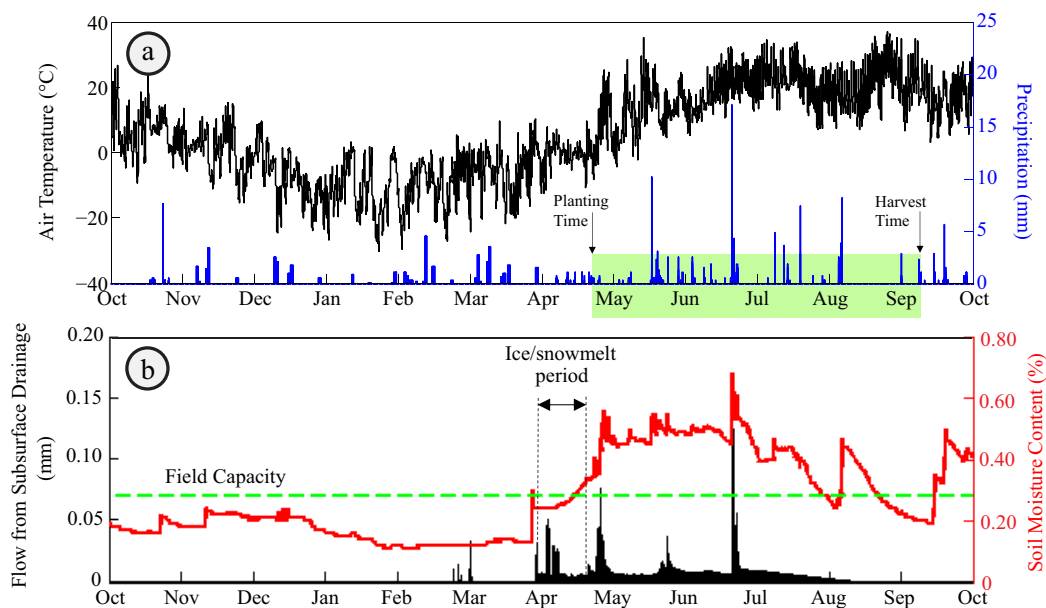
Figure 3. Detailed data at the 11.41 ha Discovery Farms Minnesota experimental site Stearns (ST1) near the Redwood basin used to parameterize the SAS function displayed in Figure 4. (a) Precipitation and air temperature, and (b) subsurface drainage flow and soil moisture content for the water year 2013. All data were measured in 15 min increments, except precipitation from November to April that is not available at this site and the daily data shown above were obtained from the nearest National Weather Service station.

2. *Snowmelt season* (*April*). Shortly after the snowmelt begins (usually in April depending on the climatic condition and lasting for at most three weeks), the soil moisture gradually increases until it goes beyond the field capacity and the subsurface tiles start draining water from the soil, which includes a mixture of new and prestored water particles. Therefore, the random-sampling scheme is considered for this season.

3. *Growing season* (*May–July*). The major contribution to streamflow from subsurface tile drainage is observed in May, June, and July when the subsurface has large capacity for water storage as inferred from its high soil moisture above field capacity (see Figure 3b), resulting in a high contribution of young or fast flushed-out event-based water particles to streamflow. Comparing the chemographs and stream-flow hydrographs in other tile-drained agricultural systems also indicate macropore flow quickly carries event water and water-borne chemicals to the receiving tile drainage networks under similar conditions [e.g., *Richard and Steenhuis*, 1988; *Gall et al.*, 2011]. Thus, a SAS function with higher preference to the younger ages is assumed for this season.

4. *Senescence season* (*August*). In August, the soil moisture is relatively high, but not as high as the May-June-July period because the soil moisture in excess of field capacity has already been removed by the drainage system as well as the growing crops' transpired water. Thus the soil has available volume for water storage, and less tile drainage is observed from the subsurface system compared to May, June, and July, prompting us to assume a SAS function with equal likelihood of age sampling.

5. *Fall season* (*September–November*). Last, during September–November, the soil moisture gradually decreases and almost no discharge is observed from the drainage system, except in those times experiencing very intense rainfall events. Thus, a SAS function with preference to the older ages is selected for this season, but the preference is smaller than that for the winter season because the water particles entering from the new precipitation still have the chance to mix with the prestored particles.

4.1.2. Quantitative Parameterization of the SAS Functions

To convert the qualitative forms of the SAS functions discussed above into quantitative expressions, we follow the approach proposed by *van der Velde et al.* [2012] in which the SAS function is quantified in terms of the cumulative probability of the residence times. Since the cumulative distribution function takes values between zero and one, a typical parameterization of the SAS function is via the Beta distribution with shape parameters α and β. In this work, we assume time-invariant SAS functions where the parameter β is set to 1

for all seasons during both the BULC (pre-1975) and ALUC (post-1975) periods to ensure a monotonic shape for the beta distribution so that the SAS function gives preference to only one type of sampling ages, i.e., no simultaneous high preference is given to both young and old particles, which would not be physically realistic. This is consistent with the shape of the SAS functions inferred from long-term hydrochemical data sets in highly monitored settings [e.g., *Harman*, 2015; *Benettin et al.*, 2015b]. The parameter α, however, has to be determined for all seasons and for both the BLUC and ALUC conditions.

Let us denote by $i = 1, 2, 3, 4,$ and 5, the winter, snowmelt, growing, senescence, and fall seasons, respectively, and by $j(i)$ the indices of the months belonging to season i, that is, for season $i = 1$ (winter: December–April), $j(i) = 12, 1, 2, 3$. The parameters α_i^{BLUC} and α_i^{ALUC} are determined by solving the following optimization problem:

$$Minimize: \sum_{k \in j(1)} | MTT_k^{BLUC} - MTT_k^{ALUC} | \tag{3}$$

$$Subject\ to: \beta_{i=1,\dots,5}^{BLUC} = 1,\ \beta_{i=1,\dots,5}^{ALUC} = 1, \tag{4a}$$

$$\alpha_{i=2,4}^{ALUC} = 1,\ 1 < \alpha_{i=1,5}^{ALUC} < 2,\ 0 < \alpha_{i=3}^{ALUC} < 1,\ \alpha_{i=5}^{ALUC} < \alpha_{i=1}^{ALUC} \tag{4b}$$

$$\alpha_{i=1}^{BLUC} = \alpha_{i=1}^{ALUC},\ \alpha_{i=2,\dots,5}^{BLUC} = \alpha_{i=5}^{ALUC} \tag{4c}$$

We note that $\alpha = 1$ indicates a random-sampling scheme, while $\alpha < 1$ and $\alpha > 1$ gives preference to young and old particles, respectively, as inferred qualitatively in the previous section. In essence, the above objective function (3) treats the transport mechanism during "winter" (season $i = 1$) as a constraint for the estimated MTTs. Indeed, since (1) subsurface drainage tiles are inactive during winter, and (2) the soil is frozen, hence the input precipitation (consisting of zero-age particles) has no chance to be mixed with the pre-stored water from last season(s), the mixing properties (SAS function) and the transport time scales (MTT) in the shallow subsurface layer are assumed to be the same during the BLUC and ALUC conditions. The solution of the above constrained optimization problem results in $\alpha_{i=1}^{ALUC} = 1.6$, $\alpha_{i=3}^{ALUC} = 0.5$, and $\alpha_{i=5}^{ALUC} = 1.4$, and the corresponding SAS functions are shown in Figure 4b.

To gain insight into the sensitivity of the MTTs to the assumed parameters of the SAS functions, we examined two extreme conditions, each giving preference to only young and only old particles, respectively, at all times in the ALUC period. The MTTs could increase (decrease) by 50% by switching from the seasonally parameterized SAS functions to the ones giving high preference to only old (only young) particles throughout the year. However, these are extreme and not physically meaningful parameterizations since they do not acknowledge the considerable within-year variability and are not consistent with the tile drainage observations of Figure 3b. As a final remark, it should be noted that because the parameterized SAS functions are not expressed in terms of the residence time itself, the residence time distribution cannot be directly computed from the given analytical expressions and the master equation (ME) (see equation (A2) in Appendix A) must be solved numerically. The chosen time step to update the storage while solving the mass balance equation (through a forward difference scheme) should be fine enough to achieve accurate computation of residence time probabilities. This is because the ME involves the ratios between the precipitation, discharge, evapotranspiration fluxes and storage, and if these fluxes are large enough compared to the storage, coarse time steps will result in significant numerical errors. It can be simply shown that the numerical solution of the ME using hourly time step suffices to avoid such an issue, which decreases the numerical error by 2 orders of magnitude compared to the daily time step.

4.2. Temporal Evolution of the Travel Time Statistics

By using the daily precipitation, evapotranspiration, discharge, and soil storage fluxes and parameterizing the SAS functions, the residence and forward travel time distributions are computed at a daily scale. Figures 5c and 5d show examples of such distributions conditional on time t_1: 13 September 1974 and t_2: 16 June 1993, belonging to two periods with dry and wet hydrologic conditions, respectively (Figures 5a and 5b). For each case, the impact of rainfall intermittency is clearly reflected in the nonsmoothness of the TTDs, and the location of the peaks follows that of the discharge time series. There is also a remarkable difference between these two forward TTDs with respect to the shape, number of peaks, and the obtained range of the travel times. For instance, Figures 5c and 5d show that the water particles injected at time t_2 resulted in
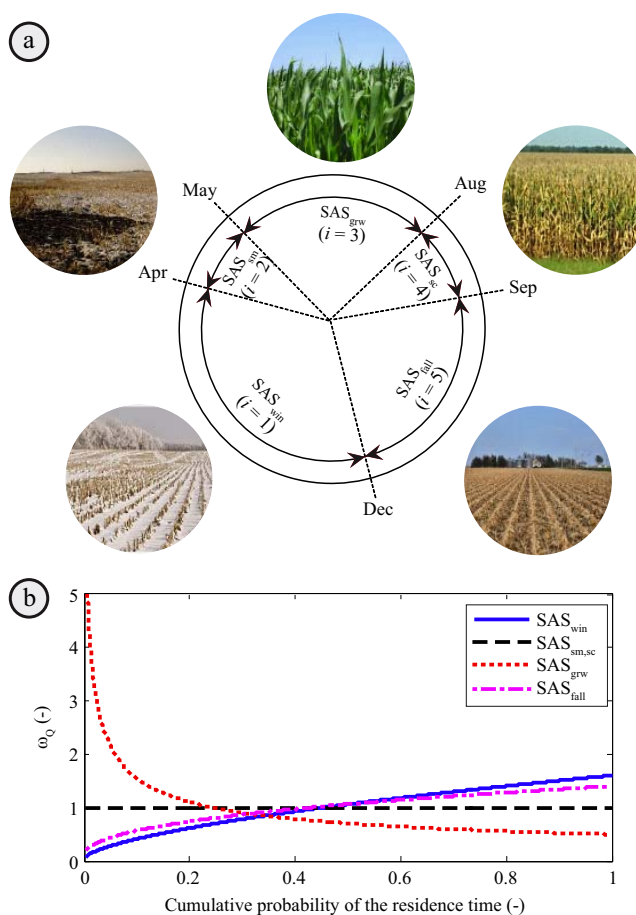
Figure 4. Parameterization of the StorAge Selection (SAS) function. (a) Qualitative inference of the type and form of the SAS functions for five distinct seasons in a year, determined by identifying the sampling mechanism in each season by the use of hydrological fluxes at a field scale (see Figure 3). SAS_{win}, SAS_{sm}, SAS_{grw}, SAS_{sc}, and SAS_{fall} represent the SAS functions corresponding to the winter ($i = 1$), snowmelt ($i = 2$), growing ($i = 3$), senescence ($i = 4$), and fall ($i = 5$) seasons, respectively. (b) Parameterized SAS functions as a Beta density function with parameters α and β. The parameter β was set to 1 for all seasons during both the BULC (pre-1975) and ALUC (post-1975) periods to ensure a monotonic shape for the beta distribution so that the SAS function gives preference to only one type of sampling ages. In the ALUC period, the parameter α was set to 1 in the snowmelt and senescence seasons (i.e., $\alpha_{i=2,4}^{ALUC}=1$) to enforce a random-sampling scheme, while during the winter, growing, and fall seasons, α was determined by solving a constrained optimization problem given in equations (3) and (4), resulting in $\alpha_{i=1}^{ALUC}=1.6$, $\alpha_{i=3}^{ALUC}=0.5$, and $\alpha_{i=5}^{ALUC}=1.4$ (see text for details).

much smaller travel times than those injected at time t_1, mainly explained by the underlying climatic and antecedent soil moisture conditions. This can be better understood by zooming into the discharge time series during the time interval around times t_1 and t_2 (Figures 5a and 5b). The plots reveal that the rainfall event at time t_2 was both preceded and followed by wet periods leading to early peaks in the forward TTD, whereas a relatively long dry period after time t_1 resulted in a much later peak in the corresponding TTD. This illustration thus demonstrates how the temporal dynamics of the precipitation and discharge time series are translated into the temporal variability of the TTDs. In addition to the forward TTDs, the residence time distributions conditional on the same times t_1 and t_2 are also shown in Figures 5c and 5d, respectively, to highlight the remarkable difference between these two distributions. First, in contrast to the forward TTDs, the residence time distributions, $p_R(t_R, t)$, contain gaps at those ages when $J(t - t_R) = 0$. Second, their temporal evolution follows the temporal dynamics of the precipitation time series. The tail of the residence time distribution, e.g., conditional on time t_2, is also three times longer than the tail of the forward TTD conditional on the same time, resulting in quite different mean residence and mean travel time.

Figure 5e further depicts the computed partition function versus the streamflow time series for the months of May, June, and July, when the drainage system greatly contributes to discharge. The partition function can be analytically derived by setting the integral of the forward TTD to 1 [see *Botter et al.*, 2010, Appendix
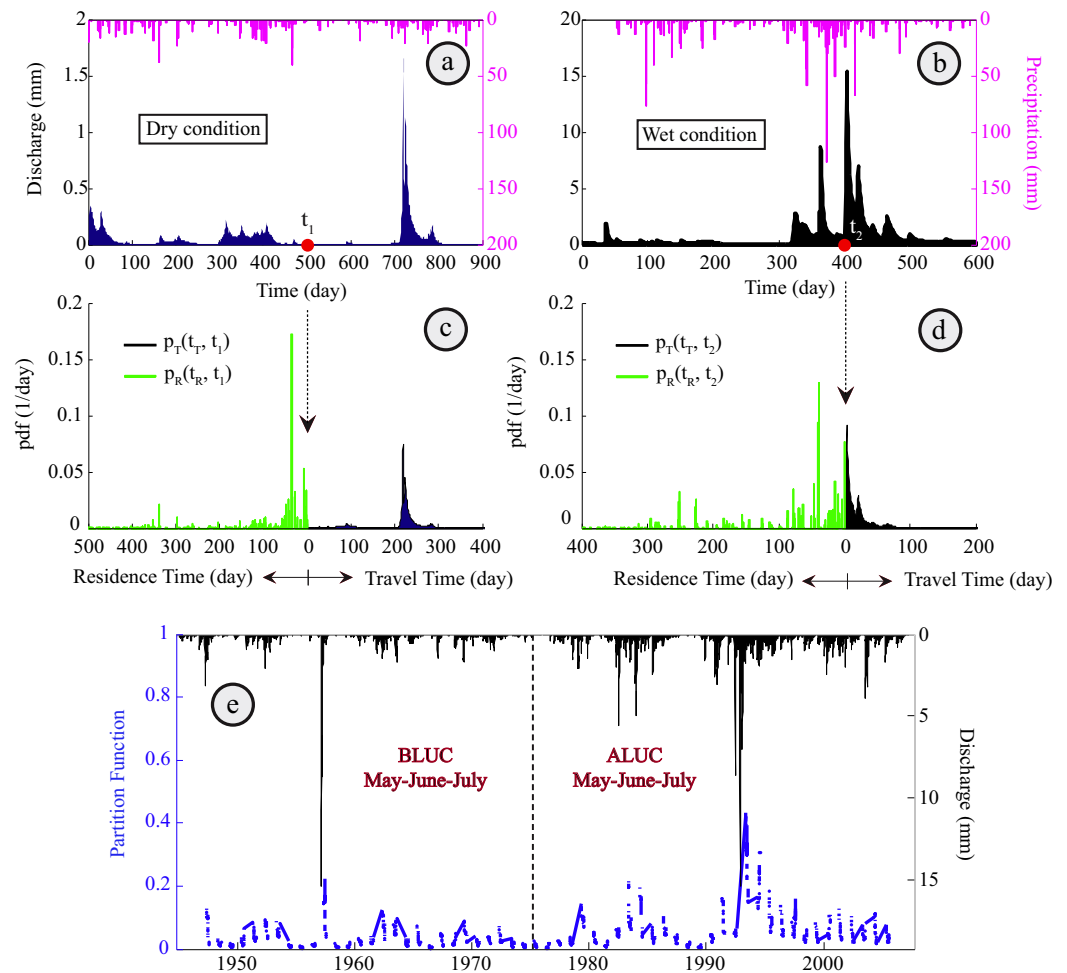
Figure 5. Residence and forward travel time distributions conditional on two times (t_1 and t_2) with different hydrologic conditions. (a and b) Observed precipitation and discharge time series around time t_1 (13 September 1974) and t_2 (16 June 1993) under dry and wet conditions, respectively. (c and d) The forward travel time distributions, $p_T(t_T, t_i)$, conditional on the injection times t_1 and t_2, show remarkable differences with respect to the shape, number of peaks, and the estimated range of the travel times. The residence time distributions, $p_R(t_R, t)$, conditional on the same times t_1 and t_2 are also shown to highlight how the travel and residence time distributions can be considerably different. (e) Partition function versus daily streamflow for the months of May, June, and July. The plot shows how the temporal evolution of the partition function follows that of the streamflow, while the increased partition function in the ALUC period is obvious compared to the BLUC one. BLUC (ALUC) denote the pre- (post-) 1975 periods.

B]. Not surprisingly, the temporal evolution of the partition function is governed by the discharge time series as the partition function at a given time gives the fraction of the injected water particles at that time leaving the system through discharge. However, the increased partition function in the ALUC period, compared to the BLUC period, is obvious (recall that the partition function ranges between 0 and 1), which is attributed to the increased discharge draining into the streams due to the subsurface drainage system.

Travel time statistics can also be tracked over time to infer how they have been changing from the BLUC to the ALUC period. Knowing the TTDs, the marginal TTDs as descriptors of the typical behavior of the system are then computed for each month by ensemble averaging the individual forward TTDs over that month from 1944 to 2007. Figure 6a shows the temporal evolution of the mean, median, 20th and 80th percentiles of the travel time for the month of June during the time window of the BLUC and ALUC periods. Time-averaged MTT has decreased by 41% from 77 days during the BLUC period to 45 days in the ALUC. This is interpreted as the result of the subsurface drainage providing faster pathways through which the drainable water (defined as the water corresponding to the soil moisture between the field capacity and saturation) can be quickly transported into the streams. The drainable water may include both the prestored water particles and the newly entered ones by most recent events, thereby the residence time of such particles
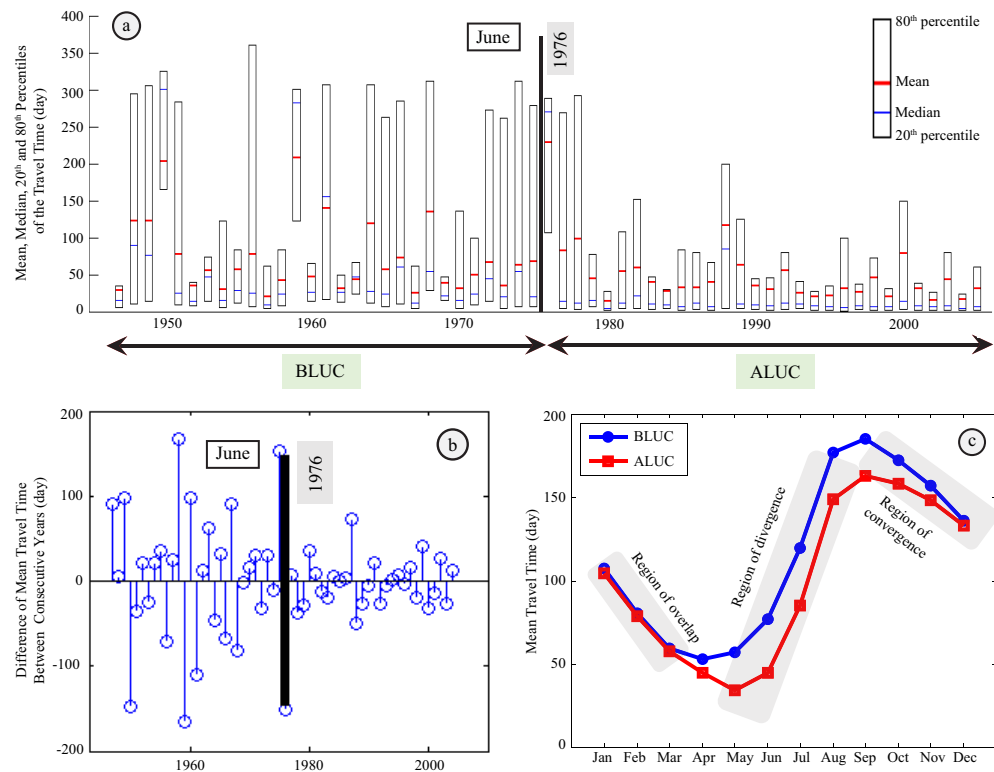
Figure 6. Temporal evolution of the travel time statistics and intra-annual variation of the MTT. (a) Mean, median, 20th and 80th percentiles of the travel time in the month of June. The time-averaged MTT indicates a reduction of 41% from 77 days during BLUC to 45 days in the ALUC period. Smaller distance between the mean, and 20th and 80th percentiles of the travel time in the ALUC period reveals significantly reduced variability in the travel times around the MTT. (b) Difference of MTT between consecutive years depicting the reduced year-to-year variation of the MTT in the ALUC period. (c) Seasonal pattern of the MTT during BLUC and ALUC periods. The ALUC curve does not exceed the BLUC curve in any month. The curves coincide during the months of December, January, February, and March, consistent with our parameterization of the SAS functions which assume that subsurface drainage system plays a minimal role in the subsurface transport during these months. Starting in April, the curves start deviating from each other while the highest difference between them shows up during the months of May–August. From September on, the effect of subsurface drainage on discharge diminishes, resulting in the gradual convergence of the BLUC and ALUC curves. BLUC (ALUC) denote the pre- (post-) 1975 periods.

would decrease while transported through the drainage system, resulting in the arrival of younger water particles to the streams compared to the undrained condition. Moreover, this plot depicts that in most years in the ALUC period the distance between the mean, and 20th and 80th percentiles of the travel time (especially the 80th percentile) is smaller than that in the BLUC period, revealing significantly reduced variability in the travel times around the MTT. Mutual comparison of the TTDs between BLUC and ALUC periods (see Figures 5c and 5d for an example) also demonstrates that the TTDs during the ALUC period are more asymmetric in shape and show considerable shorter tail than those in the BLUC period.

Figure 6b, showing the differences of MTT between consecutive years, further demonstrates that the year-to-year MTT fluctuation in the ALUC period is also much smaller compared to that of the BLUC period, implying that the system has been hydrologically "homogenized" by the subsurface drainage system and responding in a more constrained or engineered way. Indeed, subsurface drainage basically provides a condition for a more uniform system response by reducing the degree of importance of the natural variability in key hydrologic processes such as groundwater table fluctuations or variations in the unsaturated hydraulic conductivity. The homogenization of the landscape by the artificial drainage systems has been already discussed by *Basu et al*. [2011] and the above observation is consistent with the findings of *Schilling and Helmers* [2008] who explored the effect of drainage on the base flow and stormflow portion of the hydrographs as well as the characteristics of the streamflow recession after storm events. By analyzing the recession part of the hydrographs from heavily drained and less drained regions in Iowa and performing some model simulations, they concluded that the master recession curve (that is, the streamflow recession

plotted against time on a semilogarithmic scale) in intensively drained watersheds appears to indicate a linear relationship between storage and discharge compared to the less drained watersheds. This suggests that intensive subsurface drainage in such watersheds has led to the homogeneity in the dominant flow paths, resulting in a more predictable hydrologic response [*Boland-Brien et al.*, 2014]. These conclusions are also in accordance with the findings in *Foufoula-Georgiou et al.* [2015] where it was shown that the inherent nonlinearity of the daily streamflow time series in the ALUC period was considerably reduced compared to the BLUC, attributed again to a more "regularized" hydrologic response of the replumbed landscape.

4.3. Seasonal Variation of the Mean Travel Time (MTT)

Figure 6c shows the seasonal variation of the MTTs for the BLUC and ALUC periods. Some interesting features are apparent in this figure. First, both curves show an overall cyclic shape during a year which is consistent to the similar behavior found by *Heidbuchel et al.* [2012] who also obtained a sinusoidal shape for the intra-annual variation of the MTT. Second, the ALUC curve does not exceed the BLUC curve in any month. An overlap of the curves during the months of December, January, February, and March (winter season) is consistent with our parameterization of the SAS functions which assumes that the drainage system during these months plays a minimal role in the subsurface transport and, in fact, this condition formed a major component of the constrained parameter estimation problem (see equations (3) and (4a)). Third, the MTT curves begin to deviate from each other starting in April, i.e., at the beginning of the snowmelt period, with the ALUC curve remaining below the BLUC during the whole year, with the highest difference between them during the months of May–August. From September on, the effect of the drainage system on discharging water from the subsurface diminishes, resulting in the gradual convergence of the BLUC and ALUC curves. Substantial decrease in the MTT during the wet period (i.e., May-June-July), when the soil moisture exceeds the field capacity leading to drainage from subsurface tiles, might have serious implications for the water quality of the streams as the drainage system bypasses riparian buffers [*Schilling et al.*, 2015], contributing to the environmental degradation of surface waters due to eutrophication [*Ayars and Evans*, 2015].

The range of the estimated MTTs for the Redwood basin is small compared to the MTTs obtained for many other basins by using tracer or stable isotope measurements [e.g., see *McGuire and McDonnell*, 2006, Table 1]. This is partially because the MTTs were estimated by considering only the mixing processes that take place in the root zone layer, and not in the deep groundwater zone. The groundwater contribution to the travel times can be incorporated by using other approaches such as a double-storage model [*Benettin et al.*, 2013b, 2015b]. This approach partitions the total storage into the shallow subsurface and deep groundwater layers, enabling us to compute the TTDs for each layer, separately, which obviously results in much longer MTTs corresponding to the groundwater layer. However, the focus of this study was only on the transport features taking place in the root zone layer because the subsurface drainage tiles are essentially beneath this zone (and above the groundwater table), cutting off the soil top layer from the deeper zone. In addition, a few recent studies [*Kirchner*, 2009; *Birkel et al.*, 2011, *Benettin et al.*, 2015b] have also shown that the chemical response of a watershed can be considerably influenced by another storage component, referred to as residual (or passive/dead/hidden) storage, which is not hydrologically active and can result in residence times that are much longer compared to the residence times of particles belonging to dynamic storage. This is an important consideration for the transport of reactive chemicals, nitrogen, and phosphorous in the agricultural watersheds but unfortunately, it cannot be incorporated except in the presence of hydrochemical data. We understand that neglecting the residual storage, as considered in this study due to the lack of hydrochemical data, can largely impact the absolute value of the estimated MTTs. However, since the residual storage is not influenced by the dynamical hydrologic fluxes and does not directly contribute to the streamflow [*Fenicia et al.*, 2010; *Soulsby et al.*, 2011], it is assumed that this portion of the total storage is not affected by the LULC change in the Redwood basin and consequently, it does not impact the relative difference between the estimated MTTs in the BLUC and ALUC periods.

5. Sensitivity Analysis Via Numerical Simulation of Travel Times From Hillslope to Watershed Scale

Our analysis in the previous section considered the whole basin as a lumped control volume and used the available hydrologic data at the basin outlet to estimate the MTTs. This approach did not explicitly take into

account the spatial heterogeneity that is present in river basins, e.g., due to the spatially variable soil saturated hydraulic conductivity (K_{sat}). Moreover, the estimated MTTs might be very different from those that could be estimated from basins of smaller spatial scales if data were available. The goal of this section is thus to explore the following specific questions: (1) what is the sensitivity of the MTT to the spatial heterogeneity of soil characteristics that affect the mixing and transport of water and solutes throughout a catchment? and (2) what is the dependence of MTT on spatial scale and how does spatial heterogeneity control the MTTs estimated at hierarchical spatial scales of a basin? The answers to the above questions would provide insight on the reliability of the assessment of a catchment's behavior based on the data collected at the basin scale.

To this goal, a series of numerical simulations from hillslope to watershed scale were performed using a stochastic soil moisture model (see *Laio et al.* [2001] for a detailed expression of the model), which is based on the soil water balance of a hillslope in terms of precipitation, evapotranspiration, discharge, and water storage in the soil, and only considers the root zone dynamics. Daily rainfall is simulated as a Poisson process with the arrival rate λ (1/day), i.e., the average daily rainfall interarrival time (consecutive dry days separating rainy events) is $1/\lambda$ (day), and the daily rainfall depth is sampled from an exponential distribution with mean, γ (mm). Evapotranspiration is assumed to linearly increase with the soil moisture content, i.e., $ET(t) = ET_{max} (s(t) - s_{wp})/(s_{fc} - s_{wp})$, where the parameters ET_{max}, s_{fc}, and s_{wp} are assumed depending on the considered basin and soil type [see e.g., *Laio et al.*, 2001]. By assuming that the vertical flow is driven by gravity, the discharge is approximated to be proportional to a power of the soil water storage, $Q(t) = K_{sat} s(t)^c$ [*Brutsaert and Nieber*, 1977], where the exponent c depends on the soil type and can be determined by using the available look-up tables [e.g., *Laio et al.*, 2001, Table 1]. For the sake of simplicity, a uniform SAS function (i.e., random-sampling scheme) for both Q and ET is chosen while computing the TTDs.

5.1. Dependence of Hillslope Mean Travel Time (MTT) on Saturated Hydraulic Conductivity

In the first set of simulations, the Redwood basin is first decomposed into single channels and their corresponding 315 hillslopes by using the National Hydrography Dataset (NHDPlus2 released in 2012), where the hillslope or the incremental area is defined as the area draining directly into its connecting channel (see Figure 1b). The root zone depth, average daily rainfall depth, and average rainfall interarrival time are set to 1000 mm, 20 mm, and 6.6 days, respectively. The mean of the lognormal distribution from which K_{sat} is randomly generated is set to 350 mm/d and the variance is chosen such that it gives a set of bounding real-world values for K_{sat}, ranging from ~100 mm/d for clay to ~2000 mm/d for sand. Given the above parameters, the model is run for each hillslope during a time window of 20 years and the forward TTDs are then computed using the fluxes corresponding to that hillslope. Figure 7a shows the temporal variation of the MTT versus injection time for two hillslopes with minimum and maximum K_{sat}. The hillslope with the smallest K_{sat} gives higher travel times due to slow transport of water through the soil. On the contrary, MTTs relating to the hillslope with the maximum K_{sat} are much smaller as higher hydraulic conductivity facilitates rapid movement of water in the hillslope. The MTTs corresponding to all the other hillslopes (not shown here) fall between these two extreme bounds. Spatial heterogeneity of the soil K_{sat} at the hillslope scale also results in significant variation of the MTT. By time-averaging the MTT relating to each hillslope, Figure 7b shows an emergent relationship between average MTT and hillslope K_{sat}. For K_{sat} less than nearly 600 mm/d, a power law relationship ($R^2 = 0.98$) governs, while a linear relationship ($R^2 = 0.99$) holds for K_{sat} larger than 600 mm/d. A linear variation of the average MTT with relatively large K_{sat}'s (relating to loamy sand and sandy soils) can be explained as follows. As mentioned earlier, drainage from a hillslope varies as a power of water storage with the proportionality coefficient, K_{sat}, and the exponent that is dependent on the field capacity, with drainage taking place when the soil moisture exceeds the field capacity. On the other hand, the soil field capacity also decreases with increasing K_{sat}, with the rate of decrease highly dampened when K_{sat} is larger than ~500 mm/d [e.g., see *Laio et al.*, 2001, Table 1]. This suggests that when the soil K_{sat} is larger than a threshold, the resulting discharge from a hillslope is mainly governed by K_{sat} and becomes less dependent on the interplay between the field capacity and soil moisture, which in turn is reflected in the TTDs as they are strongly controlled by the hydrologic fluxes. The power law dependence of MTT on K_{sat} for K_{sat} less than 600 mm/d is harder to analytically explain as discharge is nonlinearly dependent on both K_{sat} and field capacity and the emergence of such a relationship requires further study.
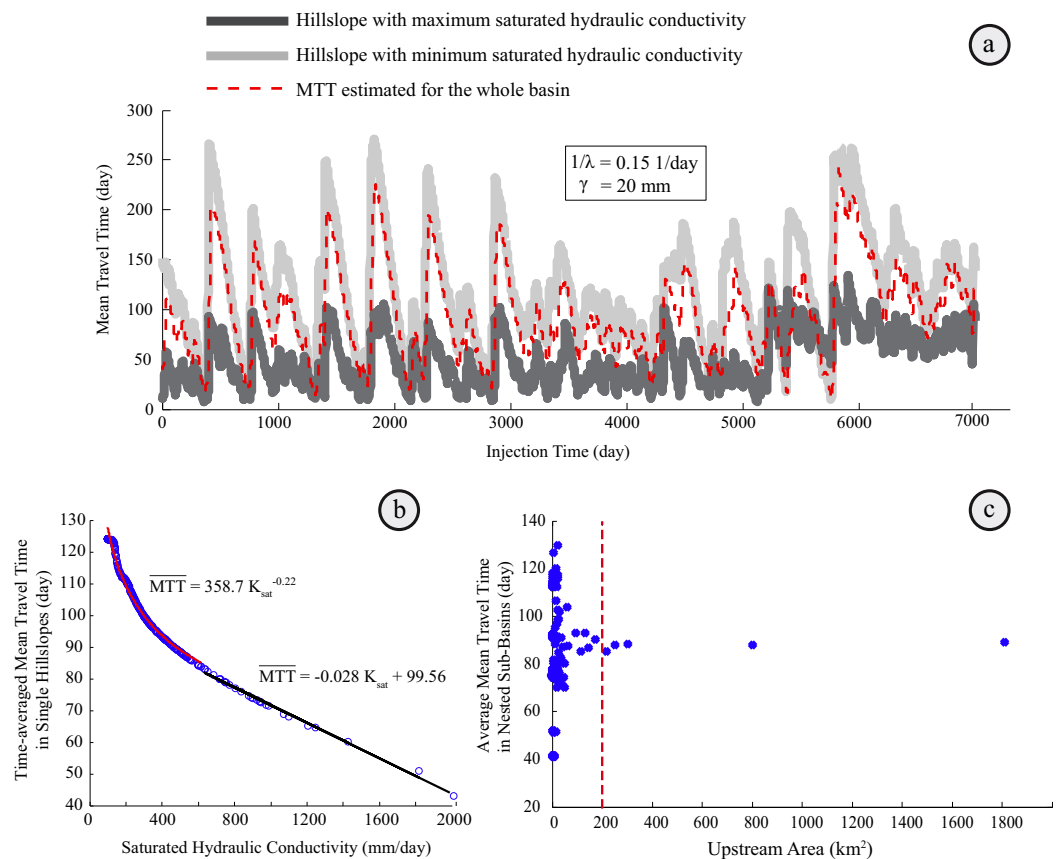
Figure 7. The effect of soil saturated hydraulic conductivity (K_{sat}) and spatial scale on the MTT. (a) MTT versus injection time for two hillslopes with minimum and maximum K_{sat}, and also for the whole basin scale. The overall basin MTT was computed as the integration of the MTTs of the nested subbasins along the river network. (b) Time-averaged MTT versus soil K_{sat}, approximated by power law and linear relationships for soil saturated hydraulic conductivity less than and larger than 600 mm/d, respectively. (c) Time-averaged MTT versus upstream area estimated for all nested subbasins. The MTT shows independence with respect to the catchment size for spatial scales approximately larger than 200 km^2.

5.2. Dependence of Mean Travel Time (MTT) on Spatial Scale

While the dependence of hydrologic response on the basin size has been investigated by several studies [e.g., *Sivapalan et al.*, 2002; *Botter and Rinaldo*, 2003; *Chen et al.*, 2015], only a few studies have explored the dependence of the MTT on the catchment size using limited tracer data gathered in the field [e.g., *McGlynn et al.*, 2003; *McGuire et al.*, 2005; *Hrachowitz et al.*, 2010a]. The dependence of MTT on spatial scale is examined here by coupling the hillslope numerical simulations discussed in the previous section with a flow routing model along the river network of the Redwood basin. In the NHD data set, each channel is labeled by its unique position in the network (immediately upstream and downstream joining channels), hence the whole network connectivity information is known. In addition, the topographic and geometric properties of the channels including the length, slope, and incremental area can be directly extracted from this data set or computed using the spatial analysis tools available in ArcGIS. Having delineated the river network topology and geomorphologic properties, the numerical model is run for each hillslope separately, and then the outflows from all hillslopes are routed through the channel network until the total water mass leaves the watershed. Then the whole upstream area of each subbasin is considered as a single CV and the travel time analysis is performed by using the routed fluxes at the end of that subbasin. Since the transport time scale in the river channels is typically smaller than that of the hillslopes (order of hours instead of days), the daily outflow from a hillslope is first distributed uniformly over a day to obtain an hourly outflow and then it is used as input for flow routing. The applied flow routing scheme is based on the numerical solution of the coupled mass and momentum conservation equations for each channel using the real geometric and topographic attributes of the channels, thereby real velocities in the river network (for more detail on the formulation of the routing model, see *Mantilla et al.* [2006]).

Figure 7a shows the MTTs estimated by considering the whole basin as a single CV, indicating that they fall between the MTTs computed for single hillslopes with maximum and minimum K_{sat}. This highlights that the effect of spatial heterogeneity at small scales on the MTTs diminishes when the spatial scale increases and integration of catchment physical properties takes place [see also *Kirchner et al.*, 2010; *Ayalew et al.*, 2014]. The dependency of the MTT on the spatial scale can be examined by plotting the time-averaged MTT relating to every subcatchment against upstream area. As Figure 7c shows, there is no evident correlation between the MTT and catchment size at small scales. By using the tracer or stable isotope of water to estimate the mean residence time in a wide range of catchments from 0.026 to 62.42 km^2, *McGlynn et al.* [2003] and *McGuire et al.* [2005] also found no correlation between the catchment area and the estimated mean residence time where some larger catchments even had smaller mean residence time than the smaller catchments. However, our numerical simulations indicate that after the spatial scale of nearly 200 km^2, the MTT gradually converges to a constant value indicating independence with respect to scale. Such a behavior and scale independence at approximately 200 km^2 is similar to the results obtained by the field experiments of *Hrachowitz et al.* [2010a] who estimated the MTT from isotopic data in 20 nested catchments in North East Scotland, ranging from 1 to 1700 km^2. This suggests that there exists a characteristic scale above which homogenization of smaller scale heterogeneities takes place rendering MTT independent of scale. What exactly determines the magnitude of this characteristic scale is unclear and requires further study.

6. Summary and Conclusions

The purpose of this study was to quantify the impact of climate and land use land-cover (LULC) change, particularly the effect of extensive agricultural subsurface drainage, on the water cycle dynamics of intensively managed landscapes employing the theory of time-variant travel time distributions (TTDs) within a stochastic Lagrangian transport formulation. By applying the methodology to the Redwood River Basin in the midwestern U.S., where extensive expansion of subsurface tile drainage and a change in the daily hydrologic response have been documented in the post-1975 period, the following conclusions are made:

1. Travel time analysis showed that the mean travel time (MTT) has considerably decreased post-1975, compared to the pre-1975 period, during all months with the maximum reduction during the growing season (e.g., reduction by 41% in the month of June). This is attributed to the intensification of tile drainage that can effectively extract the excess soil moisture from the subsurface by providing extra pathways through which water is delivered to the streams much faster compared to the natural transport within the soil matrix.
2. The year-to-year variability of the MTT was also found to be highly reduced in the presence of extensive subsurface tile drainage, indicating that the "filtering" of the natural heterogeneity via the artificially replumbed landscape results in a time-space homogenization of the hydrologic response and an overall system that responds to climatic variability in a more predictable way.
3. The spatial heterogeneity of the soil properties, e.g., saturated hydraulic conductivity, was found to strongly affect the MTTs at the hillslope scale; however, as the integration of the catchment's physical properties took place along the river network, the influence of the subcatchment spatial heterogeneity was reduced. In fact, the MTT became independent of catchment size for scales larger than approximately 200 km^2, revealing that at this scale the hierarchical network-structured heterogeneities are filtered out and the overall basin MTT approaches the average MTT estimated at the hillslope scales.

Overall, our work puts forth the hypothesis that aspects of internal landscape plumbing can be estimated with hydrologic time series data in the absence of hydrochemical data in spite of the uncertainty in the estimation of the StorAge Selection (SAS) functions. Even with increased collection of hydrochemical data and higher spatial resolution of these data due to advances in remote-sensing technology, such hydrochemical data cannot be historically reconstructed where they did not exist. Our study provides one approach to examine the relative effect of land use and other landscape changes based on more widely and historically available data. Specifically, even if the absolute values of the travel and residence times is not possible to obtain accurately, the detection and physical interpretation of system changes resulting from climatic and/

or human alterations might still be feasible. Altered water pathways, and especially shortened residence time of water in the natural soil matrix, can have significant impacts on biochemical processes and thus water quality of the receiving streams. Thus, further work and data will be required to refine our analysis and interpretations.

Appendix A: Derivation of Analytical Expressions for the Residence and Travel Time Distributions

Explicit expressions for the residence time distribution $p_R(t_R, t)$, and the forward and backward travel time distributions, $p_T(t_T, t_i)$ and $p'_T(t_T, t_e)$, respectively, are derived by solving three independent equations [*Botter et al.*, 2011]. The first relationship known as the *Niemi*'s [1977] equation is expressed as

$$Q(t)p'_T(t-t_i, t) = J(t_i)\theta(t_i)p_T(t-t_i, t_i) \tag{A1}$$

where $Q(t)$ is streamflow, $J(t)$ is precipitation, and $\theta(t)$ is the partition function. The right-hand side represents the fraction of water particles injected at time t_i leaving the control volume (CV) via Q at time t, and the left-hand side describes the fraction of the discharge sampled at time t composed of those particles entered at time t_i. The second equation, known as the master equation (ME), is expressed as

$$\frac{\partial(S(t)p_{RT}(t_R, t))}{\partial t} = -S(t)\frac{\partial(p_{RT}(t_R, t))}{\partial t_R} - Q(t)p'_T(t_R, t) - ET(t)p'_{ET}(t_R, t) \tag{A2}$$

where $S(t)$ is soil storage and $ET(t)$ is evapotranspiration. The left-hand side of the above equation explains the temporal change of the water particles in storage having ages t_R at time t, and the right-hand side consists of three terms responsible for the change of the age of water particles. The first term relates to the natural aging of the water particles as time progresses. The second term shows the fraction of the ages in storage that are sampled by Q at time t, and the third term is similar to the second one, but relevant to those ages leaving the CV at time t via ET. To close the above formulation, the third independent equation is given by writing the relationship between the backward and residence time distributions as

$$p'_T(t_T, t_e) = p_{RT}(t_T, t_e)\omega_Q(t_T, t_e) \tag{A3}$$

$$p'_{ET}(t_T, t_e) = p_{RT}(t_{ET}, t_e)\omega_{ET}(t_{ET}, t_e) \tag{A4}$$

where ω_Q and ω_{ET} are called the *SAS functions*. By substituting the backward distributions from equations (A3) and (A4) into equation (A2), a quasi-linear partial differential equation is derived which can be solved analytically for the residence time distribution, expressed as

$$
\begin{aligned}
p_{RT}(t_R, t) = &\frac{J(t-t_R)}{S(t-t_R)} \\
&\cdot \exp\left\{\int_{t-t_R}^{t}\frac{Q(x)[1-\omega_Q(t_R-t+x, x)]}{S(x)}dx\right\} \cdot \exp\left\{\int_{t-t_R}^{t}\frac{ET(x)[1-\omega_{ET}(t_R-t+x, x)]}{S(x)}dx\right\}
\end{aligned} \tag{A5}
$$

and by inserting equation (A5) into equation (A3) and then using equation (A1), the backward and forward distributions can be derived as

$$
\begin{aligned}
p'_T(t_T, t_e) = &\frac{J(t_e-t_T)\omega_Q(t_T, t_e)}{S(t_e-t_T)} \\
&\cdot \exp\left\{\int_{t_e-t_T}^{t_e}\frac{Q(x)[1-\omega_Q(t_T-t_e+x, x)]}{S(x)}dx\right\} \cdot \exp\left\{\int_{t_e-t_T}^{t_e}\frac{ET(x)[1-\omega_{ET}(t_T-t_e+x, x)]}{S(x)}dx\right\}
\end{aligned} \tag{A6}
$$

$$
\begin{aligned}
p_T(t_T, t_i) = &\frac{Q(t_i+t_T)\omega_Q(t_T, t_T+t_i)}{S(t_i)\theta(t_i)} \\
&\cdot \exp\left\{\int_{t_i}^{t_i+t_T}\frac{Q(x)[1-\omega_Q(x-t_i, x)]-J(x)}{S(x)}dx\right\} \cdot \exp\left\{\int_{t_i}^{t_i+t_T}\frac{ET(x)[1-\omega_{ET}(x-t_i, x)]-J(x)}{S(x)}dx\right\}
\end{aligned} \tag{A7}
$$

Appendix B: StorAge Selection (SAS) Function Development

Botter et al. [2011] introduced the first representation of the SAS function called the *age function* (or *absolute* SAS function), which is a function of the travel time, hence its shape might vary greatly from one catchment to another. For practical purposes, this makes the comparison between different catchments challenging because they might span a completely different range of travel times, but follow a similar underlying mixing mechanism. To overcome this issue, *van der Velde et al.* [2012] proposed the second generation of the SAS function called *Storage Outflow Probability (STOP) function* (or *fractional* SAS function), which is a function of the cumulative probability of the residence time distribution, $P_R(t_R, t)$, having a value between 0 (indicative of the youngest water particles) and 1 (indicative of the oldest water particles). The main advantage of the STOP function with respect to the age function is that the STOP function is a probability distribution integrating into 1 and thus can be parameterized by the existing theoretical distributions to simulate various types of the sampling mechanism [e.g., *van der Velde et al.*, 2012, 2014]. *Harman* [2015] also proposed another form of such functions, named *ranked* SAS functions, which are expressed in terms of the ranked storage, i.e., $S_R(t_R, t) = P_R(t_R, t) \cdot S(t)$, rather than the cumulative probability of the residence times. Correspondingly, the ME can be reformulated by this ranked storage and the relevant ranked SAS function might be used as a tool to explicitly demonstrate the effect of the time-varying storage volume on the age selection. Availability of long time series of high-resolution hydrochemical data for input and output fluxes is necessary for inferring the appropriate form of the SAS function for a catchment of interest, which is usually a limiting factor in practical applications. Regardless of the challenges involved in calibrating the SAS function, when its appropriate form (constant or variable in time) is known for a catchment, the water and solute transport can be properly characterized in a stochastic way by the relevant residence and travel time distributions [*Rinaldo et al.*, 2015].

Appendix C: On the Planting Time and Time-Varying Crop Coefficient Curve

The data presented by *Cardwell* [1982, Table 1] was used to assign the corn planting time between 1930s and 1979. The source of this information was the State and Federal Crop and Livestock Reporting Service publications, Soil Conservation Service statistics and USDA Fertilizer Situation reports. According to this data, the corn planting time did not appreciably change from 1930s to mid-1960s. It started on 21 May and then shifted to 13 and 11 May during 1960s and 1975–1979, respectively (note that these dates are averages over the relating period). After 1979, the corn planting time was determined based on the data provided by the USDA, Statistical Service [*USDA*, 2015]. Similarly, the harvesting time can be extracted from the same database, and the duration of different growing stages is set to those recommended by *Hinck* [2008] for the Southern Minnesota. The planting/harvesting time is reported for the whole Minnesota State (rather
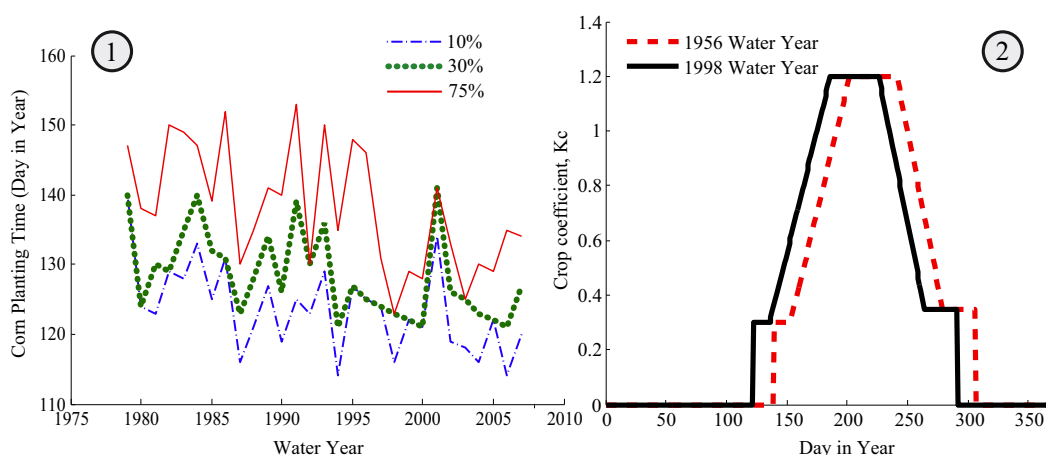

Figure C1. Temporal change in the corn planting time and crop coefficient curve. (1) Corn planting time (day of the year) in the 1979–2007 period. The trend to earlier planting times is attributed to the effectiveness of the subsurface drainage system to drain the soil. The fluctuations in the planting time arise from different climatic conditions from one year to another affecting the suitable time for planting. (2) Corn coefficient curve corresponding to two example water years 1956 and 1998 in the BLUC and ALUC periods, respectively, showing 17 days shift to earlier planting time from the water year of 1956 to 1998 with nearly the same total annual precipitation depths.

than for separate subbasins or counties) when certain percentages of these operations are complete across the State. For instance, beginning dates indicate when planting or harvesting is about 5% complete and ending dates show when operations are about 95% complete. Figure C1(1) illustrates the temporal change in the average planting time when 10, 30, and 75% of the whole State of Minnesota is planted by corn. The common observation from all curves is the overall decreasing trend in the planting time revealing the effectiveness of the subsurface drainage system in facilitating earlier planting, while the fluctuations obviously arise from different climatic conditions from 1 year to another affecting the suitable time for planting. For our analysis, we choose the curve showing the average planting time when 30% of the agricultural lands are planted because the planting time in 1979 shown by this curve is close enough to the one reported by *Cardwell* [1982]. In addition, since the Redwood basin is located in the southern third of the Minnesota reaching warm temperature earlier than the northern regions, it is reasonable to consider this basin among those 30% areas in the State where the soil temperature gets high enough so that planting can be initiated. Having extracted the planting and harvesting times using the above information, the crop coefficient curve can then be constructed for each water year, separately. Figure C1(2) shows the corn coefficient curve corresponding to two example water years 1956 and 1998 in the BLUC and ALUC periods, respectively, showing 17 days shift to earlier planting time from the water year of 1956 to 1998.

References

Asano, Y., and T. Uchida (2012), Flow path depth is the main controller of mean base flow transit times in a mountainous catchment, *Water Resour. Res.*, *48*, W03512, doi:10.1029/2011WR010906.

Ayalew, T. B., W. F. Krajewski, and R. Mantilla (2014), Connecting the power-law scaling structure of peak-discharges to spatially variable rainfall and catchment physical properties, *Adv. Water Resour.*, *71*, 32–43.

Ayars, J. E., and R. G. Evans (2015), Subsurface drainage: What's next?, *Irrig. Drain.*, *64*, 378–392.

Basu, N. B., S. E. Thompson, and P. S. C. Rao (2011), Hydrologic and biogeochemical functioning of intensively managed catchments: A synthesis of top-down analyses, *Water Resour. Res.*, *47*, W00J15, doi:10.1029/2011WR010800.

Benettin, P., A. Rinaldo, and G. Botter (2013a), Kinematics of age mixing in advection-dispersion models, *Water Resour. Res.*, *49*, 8539–8551, doi:10.1002/2013WR014708.

Benettin, P., Y. Velde, S. E. Zee, A. Rinaldo, and G. Botter (2013b), Chloride circulation in a lowland catchment and the formulation of transport by travel time distributions, *Water Resour. Res.*, *49*, 4619–4632, doi:10.1002/wrcr.20309.

Benettin, P., A. Rinaldo, and G. Botter (2015a), Tracking residence times in hydrological systems: Forward and backward formulations, *Hydrol. Processes*, *29*, 5203–5213, doi:10.1002/hyp.10513.

Benettin, P., J. W. Kirchner, A. Rinaldo, and G. Botter (2015b), Modeling chloride transport using travel time distributions at Plynlimon, wales, *Water Resour. Res.*, *51*, 3259–3276, doi:10.1002/2014WR016600.

Birkel, C., C. Soulsby, and D. Tetzlaff (2011), Modelling catchment-scale water storage dynamics: Reconciling dynamic storage with tracer-inferred passive storage, *Hydrol. Processes*, *25*(25), 3924–3936.

Birkel, C., C. Soulsby, D. Tetzlaff, and S. Dunn (2012), High-frequency storm event isotope sampling reveals time-variant transit time distributions and influence of diurnal cycles, *Hydrol. Processes*, *26*(2), 308–316, doi:10.1002/hyp.8210.

Blann, K. L., J. L. Anderson, G. R. Sands, and B. Vondracek (2009), Effects of agricultural drainage on aquatic ecosystems: A review, *Crit. Rev. Environ. Sci. Technol.*, *39*(11), 909–1001.

Boland-Brien, S. J., N. B. Basu, and K. E. Schilling (2014), Homogenization of spatial patterns of hydrologic response in artificially drained agricultural catchments, *Hydrol. Processes*, *28*(19), 5010–5020.

Botter, G., and A. Rinaldo (2003), Scale effect on geomorphologic and kinematic dispersion, *Water Resour. Res.*, *39*(10), 1286, doi:10.1029/2003WR002154.

Botter, G., T. Settin, M. Marani, and A. Rinaldo (2006), A stochastic model of Nitrate transport and cycling at basin scale, *Water Resour. Res.*, *42*, W04415, doi:10.1029/2005WR004599.

Botter, G., E. Bertuzzo, and A. Rinaldo (2010), Transport in the hydrologic response: Travel time distributions, soil moisture dynamics, and the old water paradox, *Water Resour. Res.*, *46*, W03514, doi:10.1029/2009WR008371.

Botter, G., E. Bertuzzo, and A. Rinaldo (2011), Catchment residence and travel time distributions: The master equation, *Geophys. Res. Lett.*, *38*, L11403, doi:10.1029/2011GL047666.

Broxton, P. D., P. A. Troch, and S. W. Lyon (2009), On the role of aspect to quantify water transit times in small mountainous catchments, *Water Resour. Res.*, *45*, W08427, doi:10.1029/2008WR007438.

Brutsaert, W., and J. L. Nieber (1977), Regionalized drought flow hydrographs from a mature glaciated plateau, *Water Resour. Res.*, *13*(3), 637–643.

Cardwell, V. (1982), Fifty years of Minnesota corn production: Sources of yield increase, *Agron. J.*, *74*(6), 984–990.

Chapman, A., I. D. Foster, J. Lees, and R. Hodgkinson (2005), Sediment delivery from agricultural land to rivers via subsurface drainage, *Hydrol. Processes*, *19*(15), 2875–2897.

Chen, B., W. F. Krajewski, X. Zhou, and M. J. Helmers (2015), Organized variability of surface runoff responses across neighboring hillslopes in Iowa, *J. Hydrol.*, *523*, 1−13.

Clement, J.-C., L. Aquilina, O. Bour, K. Plaine, T. P. Burt, and G. Pinay (2003), Hydrological flowpaths and nitrate removal rates within a riparian floodplain along a fourth-order stream in Brittany (France), *Hydrol. Processes*, *17*(6), 1177–1195.

Cornaton, F., and P. Perrochet (2006), Groundwater age, life expectancy and transit time distributions in advective–dispersive systems: 1. Generalized reservoir theory, *Adv. Water Resour.*, *29*(9), 1267–1291, doi:10.1016/j.advwatres.2005.10.009.

Dagan, G. (1989), *Flow and Transport in Porous Formations*, Springer, N. Y.

Dahl, T. E. (2000), Status and trends of wetlands in the conterminous united states 1986 to 1997, U.S. Fish and Wildlife Serv., Washington, D. C.

Dusek, J., T. Vogel, and M. Sanda (2012), Hillslope hydrograph analysis using synthetic and natural oxygen-18 signatures, *J. Hydrol.*, *475*, 415–427.

Fenicia, F., S. Wrede, D. Kavetski, L. Pfister, L. Hoffmann, H. H. G. Savenije, and J. J. McDonnell (2010), Assessing the impact of mixing assumptions on the estimation of streamwater mean residence time, *Hydrol. Processes*, *24*, 1730–1741, doi:10.1002/hyp.7595.

Fiori, A., and D. Russo (2008), Travel time distribution in a hillslope: Insight from numerical simulations, *Water Resour. Res.*, *44*, W12426, doi: 10.1029/2008WR007135.

Fiori, A., and D. Russo (2013), Numerical experiments on the age of seasonal rain water in hillslopes, *Proc. Environ. Sci.*, *19*, 331–340.

Foufoula-Georgiou, E., Z. Takbiri, J. A. Czuba, and J. Schwenk (2015), The change of nature and the nature of change in agricultural landscapes: Hydrologic regime shifts modulate ecological transitions, *Water Resour. Res.*, *51*, 6649–6671, doi:10.1002/2015WR017637.

Fraser, H., R. Fleming, and P. Eng (2001), *Environmental Benefits of Tile Drainage*, Prepared for LICO, Land Improvement Contractors of Ontario, Ridgetown Coll., Univ. of Guelph, Guelph, Ont.

Gall, H. E., S. A. Sassman, L. S. Lee, and C. T. Jafvert (2011), Hormone discharges from a Midwest tile-drained agroecosystem receiving animal wastes, *Environ. Sci. Technol.*, *45*(20), 8755–8764.

Gelfand, I., R. Sahajpal, X. Zhang, R. C. Izaurralde, K. L. Gross, and G. P. Robertson (2013), Sustainable bioenergy production from marginal lands in the US Midwest, *Nature*, *493*(7433), 514–517.

Ginn, T. R. (1999), On the distribution of multicomponent mixtures over generalized exposure time in subsurface flow and reactive transport: Foundations, and formulations for groundwater age, chemical heterogeneity, and biodegradation, *Water Resour. Res.*, *35*(5), 1395–1407.

Groisman, P. Y., R. W. Knight, T. R. Karl, D. R. Easterling, B. Sun, and J. H. Lawrimore (2004), Contemporary changes of the hydrological cycle over the contiguous United States: Trends derived from in situ observations, *J. Hydrometeorol.*, *5*(1), 64–85.

Groisman, P. Y., R. W. Knight, and T. R. Karl (2012), Changes in intense precipitation over the central United States, *J. Hydrometeorol.*, *13*(1), 47–66.

Harman, C. J. (2015), Time-variable transit time distributions and transport: Theory and application to storage-dependent transport of chloride in a watershed, *Water Resour. Res.*, *51*, 1–30, doi:10.1002/2014WR015707.

Heidbuchel, I., P. A. Troch, S. W. Lyon, and M. Weiler (2012), The master transit time distribution of variable flow systems, *Water Resour. Res.*, *48*, W06520, doi:10.1029/2011WR011293.

Heidbuchel, I., P. A. Troch, and S. W. Lyon (2013), Separating physical and meteorological controls of variable transit times in zero-order catchments, *Water Resour. Res.*, *49*, 7644–7657, doi:10.1002/2012WR013149.

Higgins, R. W., and V. E. Kousky (2013), Changes in observed daily precipitation over the United States between 1950-79 and 1980–2009, *J. Hydrometeorol.*, *14*(1), 105–121, doi:10.1175/JHM-D-12-062.1.

Hinck, P. J. (2008), Evapotranspiration measurement and modeling for annual and perennial crops in south-central Minnesota, MS thesis, Grad. Sch., Univ. of Minn., Minneapolis.

Holmes, R., and G. Robertson (1963), Application of the relationship between actual and potential evapotranspiration in dry land agriculture, *Trans. ASAE*, *6*(1), 65–67.

Hrachowitz, M., C. Soulsby, D. Tetzlaff, J. J. C. Dawson, and I. A. Malcolm (2009), Regionalization of transit time estimates in montane catchments by integrating landscape controls, *Water Resour. Res.*, *45*, W05421, doi:10.1029/2008WR007496.

Hrachowitz, M., C. Soulsby, D. Tetzlaff, and M. Speed (2010a), Catchment transit times and landscape controls: Does scale matter?, *Hydrol. Processes*, *24*(1), 117–125.

Hrachowitz, M., C. Soulsby, D. Tetzlaff, I. A. Malcolm, and G. Schoups (2010b), Gamma distribution models for transit time estimation in catchments: Physical interpretation of parameters and implications for time-variant transit time assessment, *Water Resour. Res.*, *46*, W10536, doi:10.1029/2010WR009148.

Hrachowitz, M., C. Soulsby, D. Tetzlaff, and I. A. Malcolm (2011), Sensitivity of mean transit time estimates to model conditioning and data availability, *Hydrol. Processes*, *25*(6), 980–990.

Jin, C., G. Sands, H. Kandel, J. Wiersma, and B. Hansen (2008), Influence of subsurface drainage on soil temperature in a cold climate, *J. Irrig. Drain. Eng.*, *134*(1), 83–88.

Kanwar, R. S., R. M. Cruse, M. Ghaffarzadeh, A. Bakhsh, D. Karlen, and T. B. Bailey (2005), Corn-soybean and alternative cropping systems effects on no 3-n leaching losses in subsurface drainage water, *Appl. Eng. Agric.*, *21*(2), 181–188.

Karl, T. R., R. W. Knight, D. R. Easterling, and R. G. Quayle (1996), Indices of climate change for the United States, *Bull. Am. Meteorol. Soc.*, *77*(2), 279–292, doi:10.1175/1520 0477(1996)077 < 0279:IOCCFT > 2.0.CO;2.

Kirchner, J. W. (2009), Catchments as simple dynamical systems: Catchment characterization, rainfall-runoff modeling, and doing hydrology backward, *Water Resour. Res.*, *45*, W02429, doi:10.1029/2008WR006912.

Kirchner, J. W. (2016), Aggregation in environmental systems: Seasonal tracer cycles quantify young water fractions, but not mean transit times, in spatially heterogeneous catchments, *Hydrol. Earth Syst. Sci. Discuss.*, *12*(3), 3059–3103.

Kirchner, J. W., X. Feng, and C. Neal (2000), Fractal stream chemistry and its implications for contaminant transport in catchments, *Nature*, *403*(6769), 524–527.

Kirchner, J. W., D. Tetzlaff, and C. Soulsby (2010), Comparing chloride and water isotopes as hydrological tracers in two Scottish catchments, *Hydrol. Processes*, *24*(12), 1631–1645.

Kladivko, E. J., L. C. Brown, and J. L. Baker (2001), Pesticide transport to subsurface tile drains in humid regions of North America, *Crit. Rev. Environ. Sci. Technol.*, *31*(1), 1–62.

Laio, F., A. Porporato, L. Ridolfi, and I. Rodriguez-Iturbe (2001), Plants in water-controlled ecosystems: Active role in hydrologic processes and response to water stress: II. *Probabilistic soil moisture dynamics, Adv. Water Resour.*, *24*(7), 707–723.

Mantilla, R., V. K. Gupta, and O. J. Mesa (2006), Role of coupled flow dynamics and real network structures on Hortonian scaling of peak flows, *J. Hydrol.*, *322*(1), 155–167.

McDonnell, J. J., and K. Beven (2014), Debates—The future of hydrological sciences: A (common) path forward? A call to action aimed at understanding velocities, celerities and residence time distributions of the headwater hydrograph, *Water Resour. Res.*, *50*, 5342–5350, doi:10.1002/2013WR015141.

McGlynn, B., J. McDonnell, M. Stewart, and J. Seibert (2003), On the relationships between catchment scale and streamwater mean residence time, *Hydrol. Processes*, *17*(1), 175–181.

McGuire, K., D. DeWalle, and W. Gburek (2002), Evaluation of mean residence time in subsurface waters using oxygen-18 fluctuations during drought conditions in the Midappalachians, *J. Hydrol.*, *261*(1), 132–149.

McGuire, K., J. J. McDonnell, M. Weiler, C. Kendall, B. McGlynn, J. Welker, and J. Seibert (2005), The role of topography on catchment-scale water residence time, *Water Resour. Res.*, *41*, W05002, doi:10.1029/2004WR003657.

McGuire, K. J., and J. J. McDonnell (2006), A review and evaluation of catchment transit time modeling, *J. Hydrol.*, *330*(3), 543–563.

McMillan, H., D. Tetzlaff, M. Clark, and C. Soulsby (2012), Do time-variable tracers aid the evaluation of hydrological model structure? A multi-model approach, *Water Resour. Res.*, *48*, W05501, doi:10.1029/2011WR011688.

Minnesota Pollution Control Agency (MPCA) (2007), Water, Water Types and Programs, Surface Water, Basins in Minnesota, Saint Paul. [Available at https://www.pca.state.mn.us/water/minnesota-river-basin.]

Minnesota Pollution Control Agency (MPCA) (2013), About the MPCA, News and Media, Features Stories, Report on nitrogen in surface water, Saint Paul. [Available at https://www.pca.state.mn.us/news/report-nitrogen-surface-water.]

National Oceanic and Atmospheric Administration (2015), National Climatic Data Center, Climate Data Online, Washington, D. C. [Available at https://www.ncdc.noaa.gov/cdo-web/.]

Niemi, A. J. (1977), Residence time distributions of variable flow processes, *Int. J. Appl. Radiat. Isotopes*, *28*(10), 855–860.

Pavelis, G. A. (1987), *Farm Drainage in the United States: History, Status, and Prospects*, vol. 1455, U.S. Dep. of Agric., Econ. Res. Serv., 110–136.

Queloz, P., L. Carraro, P. Benettin, G. Botter, A. Rinaldo, and E. Bertuzzo (2015), Transport of fluorobenzoate tracers in a vegetated hydrologic control volume: 2. Theoretical inferences and modeling, *Water Resour. Res.*, *51*, 2793–2806, doi:10.1002/2014WR016508.

Richard, T. L., and T. S. Steenhuis (1988), Tile drain sampling of preferential flow on a field scale, *J. Contam. Hydrol.*, *3*(2-4), 307–325.

Rinaldo, A., K. J. Beven, E. Bertuzzo, L. Nicotina, J. Davies, A. Fiori, D. Russo, and G. Botter (2011), Catchment travel time distributions and water flow in soils, *Water Resour. Res.*, *47*, W07537, doi:10.1029/2011WR010478.

Rinaldo, A., P. Benettin, C. J. Harman, M. Hrachowitz, K. J. McGuire, Y. Van der Velde, E. Bertuzzo, and G. Botter (2015), Storage selection functions: A coherent framework for quantifying how catchments store and release water and solutes, *Water Resour. Res.*, *51*, 4840–4847, doi:10.1002/2015WR017273.

Roa-García, M. C., and M. Weiler (2010), Integrated response and transit time distributions of watersheds by combining hydrograph separation and long-term transit time modeling, *Hydrol. Earth Syst. Sci.*, *14*, 1537–1549, doi:10.5194/hess-14-1537-2010.

Rodhe, A., L. Nyberg, and K. Bishop (1996), Transit times for water in a small till catchment from a step shift in the oxygen 18 content of the water input, *Water Resour. Res.*, *32*(12), 3497–3511.

Schilling, K. E., and M. Helmers (2008), Effects of subsurface drainage tiles on streamflow in Iowa agricultural watersheds: Exploratory hydrograph analysis, *Hydrol. Processes*, *22*(23), 4497–4506.

Schilling, K. E., C. F. Wolter, T. M Isenhart, and R. C. Schultz (2015), Tile drainage reduces groundwater travel times and compromises riparian buffer effectiveness, *J. Environ. Qual.*, *44*(6), 1754–1763.

Schottler, S. P., J. Ulrich, P. Belmont, R. Moore, J. Lauer, D. R. Engstrom, and J. E. Almendinger (2014), Twentieth century agricultural drainage creates more erosive rivers, *Hydrol. Processes*, *28*(4), 1951–1961.

Seeger, S., and M. Weiler (2014), Reevaluation of transit time distributions, mean transit times and their relation to catchment topography, *Hydrol. Earth Syst. Sci.*, *18* (12), 4751–4771, doi:10.5194/hess-18-4751-2014.

Sivapalan, M., C. Jothityangkoon, and M. Menabde (2002), Linearity and nonlinearity of basin response as a function of scale: discussion of alternative definitions, *Water Resour. Res.*, *38*(2), doi:10.1029/2001WR000482.

Skaggs, R., M. Breve, and J. Gilliam (1994), Hydrologic and water quality impacts of agricultural drainage?, *Crit. Rev. Environ. Sci. Technol.*, *24*(1), 1–32.

Soulsby, C., D. Tetzlaff, P. Rodgers, S. Dunn, and S. Waldron (2006), Runoff processes, stream water residence times and controlling landscape characteristics in a mesoscale catchment: An initial evaluation, *J. Hydrol.*, *325*(1), 197–221.

Soulsby, C., K. Piegat, J. Seibert, and D. Tetzlaff (2011), Catchment scale estimates of flow path partitioning and water storage based on transit time and runoff modelling, *Hydrol. Processes*, *25*(25), 3960–3976.

Spaling, H., and B. Smit (1995), A conceptual model of cumulative environmental effects of agricultural land drainage, *Agric. Ecosyst. Environ.*, *53*(2), 99–108.

Tetzlaff, D., J. Seibert, K. J. McGuire, H. Laudon, D. A. Burns, S. M. Dunn, and C. Soulsby (2009a), How does landscape structure influence catchment transit time across different geomorphic provinces?, *Hydrol. Processes*, *23*, 945–953, doi:10.1002/hyp.7240.

Tetzlaff, D., J. Seibert, and C. Soulsby (2009b), Inter-catchment comparison to assess the influence of topography and soils on catchment transit times in a geomorphic province; the Cairngorm Mountains, Scotland, *Hydrol. Processes*, *23*(13), 1874–1886.

Tilman, D., C. Balzer, J. Hill, and B. L. Befort (2011), Global food demand and the sustainable intensification of agriculture, Proc. *Natl. Acad. Sci.*, *108*(50), 20,260–20,264.

Tomer, M., D. Meek, D. Jaynes, and J. Hatfield (2003), Evaluation of nitrate nitrogen fluxes from a tile-drained watershed in central Iowa, *J. Environ. Qual.*, *32*(2), 642–653.

Troch, P. A., G. Carrillo, M. Sivapalan, T. Wagener, and K. Sawicz (2013), Climate-vegetation soil interactions and long-term hydrologic partitioning: Signatures of catchment co-evolution, *Hydrol. Earth Syst. Sci.*, *17*, 2209–2217, doi:10.5194/hess-17-2209-2013.

Tscharntke, T., Y. Clough, T. C. Wanger, L. Jackson, I. Motzke, I. Perfecto, J. Vandermeer, and A. Whitbread (2012), Global food security, biodiversity conservation and the future of agricultural intensification, *Biol. Conserv.*, *151*(1), 53–59.

U.S. Department of Agriculture (USDA) (2015), National Agricultural Statistics Service, Data and Statistics, Quick Stats 2.0, Washington, D. C. [Available at http://quickstats.nass.usda.gov/.]

U.S. Department of Agriculture (USDA) (2015), National Resources Conservation Service, Technical Resources, MN NRCS Redwood, Washington, D. C. [Available at http://www.nrcs.usda.gov/wps/portal/nrcs/detail/mn/technical/?cid=nrcs142p2_023602.]

van der Velde, Y., P. Torfs, S. Zee, and R. Uijlenhoet (2012), Quantifying catchment-scale mixing and its effect on time-varying travel time distributions, *Water Resour. Res.*, *48*, W06536, doi:10.1029/2011WR011310.

van der Velde, Y., I. Heidbuchel, S. W. Lyon, L. Nyberg, A. Rodhe, K. Bishop, and P. A. Troch (2014), Consequences of mixing assumptions for time-variable travel time distributions, *Hydrol. Processes*, *29*, 3460–3474, doi:10.1002/hyp.10372.

Villarini, G., J. A. Smith, M. L. Baeck, R. Vitolo, D. B. Stephenson, and W. F. Krajewski (2011), On the frequency of heavy rainfall for the Midwest of the United States, *J. Hydrol.*, *400*(1-2), 103–120, doi:10.1016/j.jhydrol.2011.01.027.

Vorosmarty, C. J., and D. Sahagian (2000), Anthropogenic disturbance of the terrestrial water cycle, *BioScience*, *50*(9), 753–765.

Walter, I. et al. (2001), ASCE's Standardized Reference Evapotranspiration Equation, Watershed Management and Operations Management, 1–11, doi:10.1061/40499(2000)126.

Weiler, M., B. L. McGlynn, K. J. McGuire, and J. J. McDonnell (2003), How does rainfall become runoff? A combined tracer and runoff transfer function approach, *Water Resour. Res.*, *39*(11), 1315, doi:10.1029/2003WR002331.

Zedler, J. B. (2003), Wetlands at your service: Reducing impacts of agriculture at the watershed scale, *Frontiers Ecol. Environ.*, *1*(2), 65–72.

Zhang, Y.-K., and K. Schilling (2006), Increasing streamflow and baseflow in Mississippi river since the 1940s: Effect of land use change, *J. Hydrol.*, *324*(1), 412–422.

Zucker, L., and L. Brown (1998), Agricultural drainage: Water quality impacts and subsurface drainage studies in the Midwest, *Ohio State Univ. Extension Bull. 871*, The Ohio State University, Ohio.